EUROPEAN ORGANISATION FOR NUCLEAR RESEARCH

CERN-PPE/94-217
16 December 1994

A Measurement of the Production of $D^{*\pm}$ Mesons on the Z^0 Resonance

OPAL Collaboration

Abstract

We have studied the production of $D^{*\pm}$ mesons in a sample of 1.25 million multihadronic decays of the Z^0, in which 1969 candidates have been identified. We have determined the total multiplicity of charged D^* mesons in multihadronic Z^0 decays to be

$$\bar{n}_{Z^0 \to D^{*\pm} X} = 0.183 \pm 0.009(\text{stat}) \pm 0.007(\text{sys}) \pm 0.008(\text{ext}),$$

The last error is due to branching ratios external to this analysis.

Decays of c-quarks are separated from those of b-quarks by a combination of bottom tagging methods using leptons, jet shape variables, and lifetime information. From this we find

$$\Gamma(Z^0 \to c\bar{c})/\Gamma(Z^0 \to \text{hadrons}) = 0.142 \pm 0.008(\text{stat}) \pm 0.009(\text{sys}) \pm 0.011(\text{ext}) \ .$$

We measure the mean scaled energy of $D^{*\pm}$ mesons in primary charm events to be

$$\langle x_{c \to D^{*\pm}} \rangle = 0.515^{+0.008}_{-0.005}(\text{stat}) \pm 0.010(\text{sys}) \ .$$

Studying D^* production at very low x_{D^*} we find indications for $c\bar{c}$ production from gluon splitting and measure the mean multiplicity of this process in multihadronic Z^0 decays to be

$$\bar{n}_{g \to c\bar{c}} = 0.044 \pm 0.014(\text{stat}) \pm 0.015(\text{sys}) \ ,$$

assuming the Standard Model prediction for $\Gamma_{c\bar{c}}/\Gamma_{\text{had}}$. By comparing our observed D^* mean scaled energy with measurements at lower energies we find evidence for scaling violations.

Submitted to Zeitschrift fúr Physik

The OPAL Collaboration

R. Akers[16], G. Alexander[23], J. Allison[16], K. Ametewee[25], K.J. Anderson[9], S. Arcelli[2], S. Asai[24], A. Astbury[28], D. Axen[29], G. Azuelos[18,a], A.H. Ball[17], E. Barberio[26], R.J. Barlow[16], R. Bartoldus[3], J.R. Batley[5], G. Beaudoin[18], A. Beck[23], G.A. Beck[13], C. Beeston[16], T. Behnke[27], K.W. Bell[20], G. Bella[23], S. Bentvelsen[8], P. Berlich[10], S. Bethke[32], O. Biebel[32], I.J. Bloodworth[1], P. Bock[11], H.M. Bosch[11], M. Boutemeur[18], S. Braibant[12], P. Bright-Thomas[25], R.M. Brown[20], A. Buijs[8], H.J. Burckhart[8], R. Bürgin[10], C. Burgard[27], N. Capdevielle[18], P. Capiluppi[2], R.K. Carnegie[6], A.A. Carter[13], J.R. Carter[5], C.Y. Chang[17], C. Charlesworth[6], D.G. Charlton[8], S.L. Chu[4], P.E.L. Clarke[15], J.C. Clayton[1], S.G. Clowes[16], I. Cohen[23], J.E. Conboy[15], M. Cuffiani[2], S. Dado[22], C. Dallapiccola[17], G.M. Dallavalle[2], C. Darling[31], S. De Jong[12], L.A. del Pozo[8], H. Deng[17], M. Dittmar[4], M.S. Dixit[7], E. do Couto e Silva[12], J.E. Duboscq[8], E. Duchovni[26], G. Duckeck[8], I.P. Duerdoth[16], U.C. Dunwoody[5], P.A. Elcombe[5], P.G. Estabrooks[6], E. Etzion[23], H.G. Evans[9], F. Fabbri[2], B. Fabbro[21], M. Fanti[2], P. Fath[11], M. Fierro[2], M. Fincke-Keeler[28], H.M. Fischer[3], P. Fischer[3], R. Folman[26], D.G. Fong[17], M. Foucher[17], H. Fukui[24], A. Fürtjes[8], P. Gagnon[6], A. Gaidot[21], J.W. Gary[4], J. Gascon[18], N.I. Geddes[20], C. Geich-Gimbel[3], S.W. Gensler[9], F.X. Gentit[21], T. Geralis[20], G. Giacomelli[2], P. Giacomelli[4], R. Giacomelli[2], V. Gibson[5], W.R. Gibson[13], J.D. Gillies[20], J. Goldberg[22], D.M. Gingrich[30,a], M.J. Goodrick[5], W. Gorn[4], C. Grandi[2], E. Gross[26], J. Hagemann[27], G.G. Hanson[12], M. Hansroul[8], C.K. Hargrove[7], P.A. Hart[9], M. Hauschild[8], C.M. Hawkes[8], E. Heflin[4], R.J. Hemingway[6], G. Herten[10], R.D. Heuer[8], J.C. Hill[5], S.J. Hillier[8], T. Hilse[10], P.R. Hobson[25], D. Hochman[26], A. Höcker[3], R.J. Homer[1], A.K. Honma[28,a], R. Howard[29], R.E. Hughes-Jones[16], P. Igo-Kemenes[11], D.C. Imrie[25], A. Jawahery[17], P.W. Jeffreys[20], H. Jeremie[18], M. Jimack[1], M. Jones[6], R.W.L. Jones[8], P. Jovanovic[1], C. Jui[4], D. Karlen[6], J. Kanzaki[24], K. Kawagoe[24], T. Kawamoto[24], R.K. Keeler[28], R.G. Kellogg[17], B.W. Kennedy[20], B. King[8], J. King[13], J. Kirk[29], S. Kluth[5], T. Kobayashi[24], M. Kobel[10], D.S. Koetke[6], T.P. Kokott[3], S. Komamiya[24], R. Kowalewski[8], T. Kress[11], P. Krieger[6], J. von Krogh[11], P. Kyberd[13], G.D. Lafferty[16], H. Lafoux[8], R. Lahmann[17], W.P. Lai[19], J. Lauber[8], J.G. Layter[4], P. Leblanc[18], P. Le Du[21], A.M. Lee[31], E. Lefebvre[18], D. Lellouch[26], C. Leroy[18], J. Letts[4], L. Levinson[26], Z. Li[12], F. Liu[29], S.L. Lloyd[13], F.K. Loebinger[16], G.D. Long[17], B. Lorazo[18], M.J. Losty[7], X.C. Lou[8], J. Ludwig[10], A. Luig[10], M. Mannelli[8], S. Marcellini[2], C. Markus[3], A.J. Martin[13], J.P. Martin[18], T. Mashimo[24], W. Matthews[25], P. Mättig[3], U. Maur[3], J. McKenna[29], T.J. McMahon[1], A.I. McNab[13], F. Meijers[8], F.S. Merritt[9], H. Mes[7], A. Michelini[8], R.P. Middleton[20], G. Mikenberg[26], D.J. Miller[15], R. Mir[26], W. Mohr[10], A. Montanari[2], T. Mori[24], M. Morii[24], U. Müller[3], B. Nellen[3], B. Nijjhar[16], S.W. O'Neale[1], F.G. Oakham[7], F. Odorici[2], H.O. Ogren[12], C.J. Oram[28,a], M.J. Oreglia[9], S. Orito[24], J.P. Pansart[21], G.N. Patrick[20], M.J. Pearce[1], P.D. Phillips[16], J.E. Pilcher[9], J. Pinfold[30], D. Pitman[28], D.E. Plane[8], P. Poffenberger[28], B. Poli[2], A. Posthaus[3], T.W. Pritchard[13], H. Przysiezniak[18], M.W. Redmond[8], D.L. Rees[8], D. Rigby[1], M.G. Rison[5], S.A. Robins[13], D. Robinson[5], N. Rodning[30], J.M. Roney[28], E. Ros[8], A.M. Rossi[2], M. Rosvick[28], P. Routenburg[30], Y. Rozen[8], K. Runge[10], O. Runolfsson[8], D.R. Rust[12], M. Sasaki[24], C. Sbarra[2], A.D. Schaile[8], O. Schaile[10], F. Scharf[3], P. Scharff-Hansen[8], P. Schenk[4], B. Schmitt[3], M. Schröder[12], H.C. Schultz-Coulon[10], P. Schütz[3], M. Schulz[8], C. Schwick[27], J. Schwiening[3], W.G. Scott[20], M. Settles[12], T.G. Shears[5], B.C. Shen[4], C.H. Shepherd-Themistocleous[7], P. Sherwood[15], G.P. Siroli[2], A. Skillman[16], A. Skuja[17], A.M. Smith[8], T.J. Smith[28], G.A. Snow[17], R. Sobie[28], S. Söldner-Rembold[10], R.W. Springer[30], M. Sproston[20], A. Stahl[3], M. Starks[12],

C. Stegmann[10], K. Stephens[16], J. Steuerer[28], B. Stockhausen[3], D. Strom[19], P. Szymanski[20], R. Tafirout[18], H. Takeda[24], T. Takeshita[24], P. Taras[18], S. Tarem[26], M. Tecchio[9], P. Teixeira-Dias[11], N. Tesch[3], M.A. Thomson[15], O. Tousignant[18], S. Towers[6], M. Tscheulin[10], T. Tsukamoto[24], A. Turcot[9], M.F. Turner-Watson[8], P. Utzat[11], R. Van Kooten[12], G. Vasseur[21], P. Vikas[18], M. Vincter[28], A. Wagner[27], D.L. Wagner[9], C.P. Ward[5], D.R. Ward[5], J.J. Ward[15], P.M. Watkins[1], A.T. Watson[1], N.K. Watson[7], P. Weber[6], P.S. Wells[8], N. Wermes[3], B. Wilkens[10], G.W. Wilson[27], J.A. Wilson[1], V-H. Winterer[10], T. Wlodek[26], G. Wolf[26], S. Wotton[11], T.R. Wyatt[16], A. Yeaman[13], G. Yekutieli[26], M. Yurko[18], V. Zacek[18], W. Zeuner[8], G.T. Zorn[17].

[1]School of Physics and Space Research, University of Birmingham, Birmingham B15 2TT, UK
[2]Dipartimento di Fisica dell' Università di Bologna and INFN, I-40126 Bologna, Italy
[3]Physikalisches Institut, Universität Bonn, D-53115 Bonn, Germany
[4]Department of Physics, University of California, Riverside CA 92521, USA
[5]Cavendish Laboratory, Cambridge CB3 0HE, UK
[6]Carleton University, Department of Physics, Colonel By Drive, Ottawa, Ontario K1S 5B6, Canada
[7]Centre for Research in Particle Physics, Carleton University, Ottawa, Ontario K1S 5B6, Canada
[8]CERN, European Organisation for Particle Physics, CH-1211 Geneva 23, Switzerland
[9]Enrico Fermi Institute and Department of Physics, University of Chicago, Chicago IL 60637, USA
[10]Fakultät für Physik, Albert Ludwigs Universität, D-79104 Freiburg, Germany
[11]Physikalisches Institut, Universität Heidelberg, D-69120 Heidelberg, Germany
[12]Indiana University, Department of Physics, Swain Hall West 117, Bloomington IN 47405, USA
[13]Queen Mary and Westfield College, University of London, London E1 4NS, UK
[15]University College London, London WC1E 6BT, UK
[16]Department of Physics, Schuster Laboratory, The University, Manchester M13 9PL, UK
[17]Department of Physics, University of Maryland, College Park, MD 20742, USA
[18]Laboratoire de Physique Nucléaire, Université de Montréal, Montréal, Quebec H3C 3J7, Canada
[19]University of Oregon, Department of Physics, Eugene OR 97403, USA
[20]Rutherford Appleton Laboratory, Chilton, Didcot, Oxfordshire OX11 0QX, UK
[21]CEA, DAPNIA/SPP, CE-Saclay, F-91191 Gif-sur-Yvette, France
[22]Department of Physics, Technion-Israel Institute of Technology, Haifa 32000, Israel
[23]Department of Physics and Astronomy, Tel Aviv University, Tel Aviv 69978, Israel
[24]International Centre for Elementary Particle Physics and Department of Physics, University of Tokyo, Tokyo 113, and Kobe University, Kobe 657, Japan
[25]Brunel University, Uxbridge, Middlesex UB8 3PH, UK
[26]Particle Physics Department, Weizmann Institute of Science, Rehovot 76100, Israel
[27]Universität Hamburg/DESY, II Institut für Experimental Physik, Notkestrasse 85, D-22607 Hamburg, Germany
[28]University of Victoria, Department of Physics, P O Box 3055, Victoria BC V8W 3P6, Canada
[29]University of British Columbia, Department of Physics, Vancouver BC V6T 1Z1, Canada
[30]University of Alberta, Department of Physics, Edmonton AB T6G 2J1, Canada
[31]Duke University, Dept of Physics, Durham, NC 27708-0305, USA

[32]Technische Hochschule Aachen, III Physikalisches Institut, Sommerfeldstrasse 26-28, D-52056 Aachen, Germany

[a]Also at TRIUMF, Vancouver, Canada V6T 2A3

1 Introduction

Measurements of the production of $D^{*\pm}$ mesons in Z^0 decays allow precise tests of both the electroweak and strong interactions. They provide tags of charmed and bottom quarks which can be used to study both the partial widths of $Z^0 \to c\bar{c}$ and to determine the fragmentation function of heavy quarks. In this analysis, we use the D^* decay chain [1]

$$\begin{aligned} D^{*+} &\to D^0\pi^+ && (68.1\%) \\ &\hookrightarrow K^-\pi^+ && (4.0\%) \end{aligned}$$

which provides a clean sample of events with which to make these studies. The numbers in brackets are the branching ratio into the channel as given in [1]. Furthermore, since the D^* is reconstructed exclusively, the shape of the fragmentation function can be measured with minimal reliance on any particular model. Measurements of low energy D^* mesons can also provide information on the process of gluon splitting into a pair of heavy quarks. Comparisons of the average D^* energy with measurements at lower centre of mass energies can be used to test results of perturbative calculations [2, 3].

These measurements depend crucially on the ability to separate the contributions to the D^* sample from primary charm and bottom quark events. In this paper we use leptons from semileptonic decays of heavy quarks, the specific topology of bottom jets and the long lifetimes of bottom quarks to identify those D^* mesons which originate from bottom quarks. The separation of the bottom contribution allows us to improve significantly on the measurement of the $c \to D^*$ production. For the first time we present a measurement covering nearly the whole kinematic range of D^* mesons produced in Z^0 decays.

We start this paper by summarising the features of the OPAL detector at LEP pertinent to this analysis, and the selection of multihadronic events. The D^* selection, the method of background determination and the global efficiency correction will be discussed in Section 4. These are very similar to those described in previous OPAL publications [4, 5]. The various methods for identifying D^* mesons from bottom decays will be addressed in Section 5. The results from these different analyses will be combined in Section 5.5 and the final results derived in Section 6. We discuss the implications of the measurements of D^* production at very low energy. Comparisons of the $c \to D^*$ fragmentation function to both QCD predictions and various models are presented in Section 7. Section 8 contains our conclusions.

2 The OPAL Detector

The OPAL detector is a multi purpose detector installed at the electron positron collider LEP. The details of construction and performance are described elsewhere [6]. Here only the main components relevant for this analysis are described.

A central part of OPAL is a large system of tracking detectors, surrounding the interaction point, and contained in a magnetic field of 0.435T. It consists of a high precision silicon microvertex detector [7] first installed for the 1991 LEP run, followed by three sets of drift chambers. These consist of a vertex drift chamber, a large volume jet-type chamber and a set of chambers which measure the coordinate along the beam direction[2]. This sys-

[1] In this paper charge conjugate modes are always implied. Also, if not otherwise noted, D^*, K etc. always refer to the charged particles.

[2] The coordinate system is defined so the z-axis follows the electron beam direction and the x-y plane is perpendicular to it with the x-axis pointing roughly towards the center of the LEP ring. The polar angle θ is defined relative to the $+z$-axis, and the azimuthal angle ϕ is defined relative to the $+x$-axis.

tem of detectors is capable of determining the momenta of charged particles with a resolution $\sigma_{p_{xy}}/p_{xy} = \sqrt{0.020^2 + (0.0015 \cdot p_{xy}/(\mathrm{GeV}))^2}$ [8], where p_{xy} is measured perpendicular to the beam direction. The polar angle, θ, is determined to around 1 mrad for about 85% of all tracks in the barrel region, defined as $|\cos\theta| < 0.72$. Outside this region, the polar angle is measured with a resolution of typically 3 mrad.

Charged particles are identified by their specific energy loss dE/dx in the jet chamber. In multihadronic events, a kaon is distinguished from a pion with better than 2σ separation for tracks with at least 100 out of 159 possible dE/dx ionisation samples and momenta between 2 and 20 GeV/c. The resolution obtained in multihadronic events for minimum ionising particles with 159 ionisation samples is 3.5% [9].

Directly outside the magnet coil and the jet chamber is the presampler. This is a system of thin chambers giving information on the early shower development of charged particles and providing an additional space point for charged tracks. This is followed by an electromagnetic calorimeter system consisting of 11 704 lead glass blocks covering the solid angle up to polar angles of $|\cos\theta| = 0.98$.

The iron of the magnet return yoke surrounding the electromagnetic calorimeter is instrumented with limited streamer chambers. It is used as a hadronic calorimeter and assists in the reconstruction of muons. The muon identification system consists of barrel and endcap muon chambers covering polar angles of $|\cos\theta| < 0.985$, outside the hadron calorimeter.

3 Hadronic Event Selection and Monte Carlo Simulation

Multihadronic decays of the Z^0 are selected by placing requirements on the number of charged tracks and the amount of energy deposited in the calorimeters, as described in Reference [10]. A total of $1,245,667$ events are selected from data collected from 1990 to 1992, taken at center of mass energies between $E_{\mathrm{cm}} = 88.4$ GeV and 93.8 GeV. The efficiency for reconstructing multihadronic events is determined to be $(98.4 \pm 0.4)\%$.

In each event, charged tracks and electromagnetic clusters not associated to a charged track are combined into jets using the invariant mass algorithm with the E0 recombination scheme [11]. Within this algorithm, jets are defined by $x_{min} \equiv y_{cut} \cdot E_{vis}^2 = 49$ GeV^2, where E_{vis} is the total visible energy and y_{cut} is defined in Reference [11]. The event is divided into two hemispheres by the plane perpendicular to the direction of the thrust vector. The thrust direction is calculated from charged tracks and neutral clusters not associated to charged tracks. The primary vertex of an event is taken to be the average intersection point of the electron and positron bunches, or beam spot. This is measured using charged tracks in the OPAL data [12] with a technique that follows any significant shifts in the position during a LEP fill.

A large sample of simulated events was generated using the JETSET 7.3 Monte Carlo [13] with parameters tuned to reproduce the OPAL data [14] and using the Peterson fragmentation function [15] for c and b quarks. A Monte Carlo sample of size roughly equivalent to the data sample analysed was generated. The fragmentation parameters used were $\epsilon_{\mathrm{c}} = 0.046$ and $\epsilon_{\mathrm{b}} = 0.0057$, corresponding to a mean scaled energy, x_E, of the first rank hadron of 0.508 and 0.700 respectively. Sets of 30000 events each of $Z^0 \to c\bar{c}$ and $Z^0 \to b\bar{b}$, events each containing at least one D^* meson which decayed into the decay chain of interest, were also generated. All Monte Carlo events were subjected to a detailed detector simulation [16] and reconstructed using the same programs as used for the data. During the analysis, the differences between

the r-ϕ track parameters[3] κ,d_0 and ϕ_0 of the reconstructed tracks and those of their associated generated particles were increased by a factor of 1.4 to account for systematic misalignments in the data that are not included in the Monte Carlo simulation.

4 The D* sample

In this section we describe the selection of D^* candidates, the determination of the background and the calculation of the selection efficiency. The method used is identical to the one described in [4, 5], where additional details may be found.

4.1 Selection of D* candidates

D^* mesons are reconstructed in the decay

$$\begin{aligned} \mathrm{D}^{*+} &\rightarrow \mathrm{D}^0\pi^+ \\ &\quad\hookrightarrow \mathrm{K}^-\pi^+ \ . \end{aligned}$$

This mode allows a particularly clean signal reconstruction, because the phase space available to background processes is severely limited by the small mass difference between the D^* and the D^0.

For a charged track to be considered in the D^* reconstruction it has to pass the following track quality cuts:

- $|d_0| < 5\,\mathrm{mm}$, where d_0 is the distance of closest approach between the track and the event vertex in the r-ϕ plane;
- $|z_0| < 20\,\mathrm{cm}$, with z_0 being the distance in z between the point of closest approach in the r-ϕ plane and the event vertex;
- $p_{xy} > 150\,\mathrm{MeV/c}$, where p_{xy} is the momentum transverse to the beam direction; and
- more than 40 hits in the jet chamber.

Candidates are selected by trying all combinations of tracks which pass the above quality cuts. Two oppositely charged tracks are combined for the D^0 candidate, with one of them assumed to be a kaon, the other a pion. A third track is added as a candidate for the pion in the $\mathrm{D}^* \rightarrow \mathrm{D}^0\pi$ decay — the so-called "slow pion". Only tracks with a charge equal to that of the track presumed to be the pion in the D^0 decay are used. Such a combination is called a D^* candidate if it passes the following mass cuts:

- $1790\ \mathrm{MeV/c^2} < M_{\mathrm{D}^0}^{cand} < 1940\ \mathrm{MeV/c^2}$,
- $142\ \mathrm{MeV/c^2} < \Delta M < 149\ \mathrm{MeV/c^2}$,

where $\Delta M \equiv M_{\mathrm{D}^*}^{cand} - M_{\mathrm{D}^0}^{cand}$, and $M_{\mathrm{D}^*}^{cand}$ and $M_{\mathrm{D}^0}^{cand}$ are the masses of the D^* and D^0 candidates, respectively.

The largest source of background to the sample is random combinations of charged tracks which pass the above mass cuts. Most of these tracks are of low momentum, resulting in

[3] The r-ϕ track parameters describing a track reconstructed in the OPAL detector are κ, the curvature; d_o, the distance of closest approach to the origin in the r-ϕ plane; and ϕ_0, the azimuthal angle of the tangent to the track at the point of closest approach.

candidates at low $x_{\mathrm{D}^*} \equiv 2E_{\mathrm{D}^*}/E_{cm}$, where E_{D^*} is the measured energy of the D^* candidate. Candidates for $x_{\mathrm{D}^*} > 0.1$, well away from the D^* production threshold, are required to have three tracks with

- $p_{xy} > 250$ MeV/c .

We further reduce the background by using the fact that the D^0 is a pseudo-scalar particle which decays isotropically in its rest frame. This results in a flat distribution of $\cos\theta^*$, where θ^* denotes the decay angle between the direction of the kaon in the D^0 rest frame and the direction of the D^0 in the laboratory frame. The background events on the other hand show pronounced peaks around $\cos\theta^* = \pm 1$, with the peak at -1 growing very fast at low x_{D^*}. Thus we require

- $\begin{aligned} -4 \cdot x_{\mathrm{D}^*} < \cos\theta^* < 0.8 \quad & \text{for } x_{\mathrm{D}^*} < 0.2 \ ; \\ |\cos\theta^*| < 0.8 \quad & \text{for } 0.2 < x_{\mathrm{D}^*} < 0.5 \ ; \\ |\cos\theta^*| < 0.9 \quad & \text{for } x_{\mathrm{D}^*} > 0.5, \end{aligned}$

Finally, we use the particle identification power of the OPAL detector to identify the kaon candidate with the following cut:

- $\begin{aligned} P^{\mathrm{K}}_{\mathrm{dE/dx}} > 0.2 \quad & \text{for } x_{\mathrm{D}^*} < 0.2 \ ; \\ P^{\mathrm{K}}_{\mathrm{dE/dx}} > 0.1 \quad & \text{for } 0.2 < x_{\mathrm{D}^*} < 0.5, \end{aligned}$

where $P^{\mathrm{K}}_{\mathrm{dE/dx}}$ is the probability that the measured rate of energy loss, dE/dx, of the kaon candidate is consistent with that expected for a real kaon.

4.2 Determination of the Background

The dominant source of background in the D^* sample is random combinations of tracks passing the applied cuts. The shape is determined from the data using specially selected event samples:

- **wrong charge candidates** are selected by requiring that the charges of the two tracks from the D^0 candidate decay products are equal, and that the charge of the slow pion candidate track is of opposite sign;
- **reflected pion candidates** are constructed by selecting a slow pion candidate track from the hemisphere opposite to a normal D^0 candidate and combining them to form a D^* candidate after reflecting the pion through the origin; and
- **reflected pion wrong charge candidates**, the same as reflected pion candidates, except that the D^0 candidate is constructed from tracks of equal sign.

The remainder of the selection and reconstruction of these candidates proceeds as described in section 4.1. Monte Carlo studies indicate that all three samples describe the shape of the true Monte Carlo background equally well. We therefore combine these in order to maximise the statistics available for the background estimation. The shape of the background is parametrised in a fit to the ΔM distribution using an empirical functional form:

$$A \cdot \exp(-B \cdot \Delta M) \cdot (\Delta M/m_\pi - 1)^C, \tag{1}$$

with A, B and C as free parameters in the fit. This fit is performed separately for $x_{\mathrm{D}^*} < 0.1$, $0.1 < x_{\mathrm{D}^*} < 0.2$, $0.2 < x_{\mathrm{D}^*} < 0.5$ and $x_{\mathrm{D}^*} > 0.5$, because of the different D^* selection cuts

applied to candidates in each of these ranges. To determine the number of D^* candidates in a given bin of x_{D^*}, the resulting background form given by the fit is normalised to the signal distribution for $155 < \Delta M < 200$ MeV/c^2. The normalised background is subtracted from the signal, and the number of D^* mesons is determined in the mass window $142 < \Delta M < 149$ MeV/c^2.

Additional background comes from decays $D^* \to D^0\pi$, followed by $D^0 \to KK$ or $D^0 \to \pi\pi$, where either one of the kaons is misidentified as a pion, or one of the pions is misidentified as a kaon. Monte Carlo studies show that the contribution from these sources is $1.6 \pm 0.2\%$ of the D^* signal. The error quoted contains the statistical error from the Monte Carlo sample used to study this effect, the error due to the branching ratios used, and the systematic errors as discussed in the following section. We corrected for this by subtracting $1.6 \pm 0.2\%$ from the total measured number of D^* mesons.

In Figure 1 the ΔM spectrum is shown in four regions of x_{D^*}. Superimposed is the estimated background. The number of D^* mesons reconstructed as a function of x_{D^*} and the background are listed in Table 1.

x_{D^*}	N_{cand}	N_{D^*}	N_{bck}	ϵ_{D^*}	$(1000/N_Z) \cdot (dN_{D^*}/dx_{D^*})$
0.0-0.1	260	7. $\pm$ 16.	253. $\pm$ 16.	0.078 $\pm$ 0.016	0.7 $\pm$ 1.7 $\pm$ 1.7
0.1-0.2	1270	202. $\pm$ 36.	1068. $\pm$ 33.	0.219 $\pm$ 0.015	7.3 $\pm$ 1.4 $\pm$ 0.7
0.2-0.3	1059	440. $\pm$ 33.	619. $\pm$ 23.	0.319 $\pm$ 0.012	11.89 $\pm$ 0.82 $\pm$ 0.70
0.3-0.4	620	350. $\pm$ 25.	270. $\pm$ 11.	0.303 $\pm$ 0.011	9.12 $\pm$ 0.64 $\pm$ 0.45
0.4-0.5	390	282. $\pm$ 20.	107.1 $\pm$ 6.0	0.288 $\pm$ 0.010	7.74 $\pm$ 0.53 $\pm$ 0.33
0.5-0.6	407	289. $\pm$ 20.	117.3 $\pm$ 6.0	0.381 $\pm$ 0.010	5.99 $\pm$ 0.41 $\pm$ 0.21
0.6-0.7	251	203. $\pm$ 16.	48.7 $\pm$ 3.1	0.392 $\pm$ 0.010	4.08 $\pm$ 0.31 $\pm$ 0.12
0.7-0.8	157	136. $\pm$ 13.	21.0 $\pm$ 1.5	0.354 $\pm$ 0.010	3.03 $\pm$ 0.28 $\pm$ 0.09
0.8-0.9	63	55. $\pm$ 7.9	8.0 $\pm$ 0.5	0.366 $\pm$ 0.011	1.19 $\pm$ 0.17 $\pm$ 0.04
0.9-1.0	10	4.7 $\pm$ 3.2	5.3 $\pm$ 0.5	0.371 $\pm$ 0.015	0.10 $\pm$ 0.05 $\pm$ 0.01
Total	4487	1969. $\pm$ 68.	2486. $\pm$ 46.		

Table 1: Number of D^* candidates reconstructed (N_{cand}) as a function of x_{D^*}, together with the signal (N_{D^*}), the background (N_{bck}) and the reconstruction efficiencies (ϵ_{D^*}). The signal includes only those D^* mesons which decay through the chain $D^* \to D^0\pi$, $D^0 \to K\pi$. The error quoted for the number of D^* mesons is the total statistical error of the sample, $\sqrt{N_{D^*} + N_{bck}}$, while the error on the background includes its statistical error and the systematic error of the background determination. The efficiency and its combined statistical and systematic error are listed in the fifth column. The last column contains the total yield of D^* mesons, normalised to the number of hadronic Z^0 decays, N_Z, along with the statistical and systematic errors, respectively.

4.3 Efficiency and Systematic Errors of the D* selection

The efficiency for finding and reconstructing D^* mesons is determined from a Monte Carlo calculation and is listed in Table 1 as a function of x_{D^*}. The observed variations with x_{D^*} are due to the cuts changing with x_{D^*} and to the deterioration of the mass resolution as the energy of the D^* increases. At very low x_{D^*} the track selection efficiencies start to drop as the threshold for D^* detection at $x_{D^*} \approx 0.055$ is approached.

The error on the efficiency is caused by the finite Monte Carlo statistics available and by possible misrepresentations of the data in the Monte Carlo. Four main sources are considered: track quality cuts, $\cos\theta^*$ cuts, dE/dx cuts and mass resolution. To check the modelling of the properties in the Monte Carlo, cuts are changed over a wide range and the response in data and Monte Carlo is compared. Some small differences are observed in the impact parameter distribution, resulting in a possible relative error on the efficiency of $\pm 1\%$. The $\cos\theta^*$ cut is well described in the Monte Carlo and the differences observed between the data and Monte Carlo are used to limit any potential systematic error to less than 0.5%. The efficiency calculated for the dE/dx cut depends on the theoretical predictions and the calibration of the specific energy loss. We investigate the change in the number of D^* events reconstructed with different dE/dx cuts, and compare this to the theoretical expectation. We find that both agree very well, corresponding to a maximum possible miscalibration of dE/dx of less than one tenth of the dE/dx resolution. This leads to a systematic error of $\pm 2\%$ on the data sample with $x_{D^*} < 0.5$. Good agreement is found between the mass resolutions in data and in Monte Carlo. The systematic error assigned to this source is obtained from the largest observed deviations between data and simulation, and is found to contribute an overall error of $\pm 2.5\%$. At very low x_{D^*} detector modelling errors in the Monte Carlo become more important, as the overall efficiency decreases. We account for this by increasing the systematic errors for the different cuts roughly in step with the decrease of the individual efficiencies. We use a total error of $\pm 7\%$ for $0.1 < x_{D^*} < 0.2$, and $\pm 20\%$ for $x_{D^*} < 0.1$. Using Monte Carlo events, we have investigated a potential efficiency difference for finding D^* mesons depending on whether they originate in $Z^0 \to b\bar{b}$ or $Z^0 \to c\bar{c}$ events. The differences observed are negligible.

The other source of systematic errors in the final yield of D^* mesons is the determination of the background. Besides the statistical error on the background due to the finite number of events in the background sample, systematic differences between the estimators and the true background and possible biases in our fitting procedure introduce errors. We estimate these by repeating the analysis while using only one of the three different background samples. In addition we repeat the background subtraction method in Monte Carlo events. We find good agreement between the results of our fits and the actual number of background events in the Monte Carlo. We assign a relative systematic error of $\pm 3\%$ to the background for $x_{D^*} > 0.2$, and $\pm 5\%$ for the low x_{D^*} region, which covers the range of variation observed in the different comparisons described, and includes the effects of the limited statistics of the Monte Carlo event sample.

5 A Model Independent Investigation of the Processes c $\to$D* and b $\to$D*

The aim of the work presented in this section is an analysis of the production of D^* mesons in decays of the Z^0 which is largely independent of any assumed model for fragmentation. There are three processes by which a D^* meson may be produced at LEP: direct production from either a b or a c quark, and the production of D^* mesons from a gluon splitting into a pair of heavy quarks. In this paper four different techniques are used to tag D^* mesons from b decays:

- a method which uses leptons in the event to tag b decays;
- an artificial neural network, which uses several jet shape variables calculated in the most energetic jet which does not contain the D^*, to tag b decays;

- a technique which looks at the separation of tracks from the Z^0 decay vertex in the thrust hemisphere opposite the D^*; and

- the reconstruction of the apparent decay length significance of the D^0 candidate in the D^* candidate decay.

The number of D^* candidates tagged as coming from a b decay, N_{b-tag}, in a sample of N_{cand} events, is given by

$$\frac{N_{b-tag}}{N_{cand}} = (1 - g_{BG}) \cdot [g_b \cdot \mathcal{P}_b + g_c \cdot \mathcal{P}_c + g_g \cdot \mathcal{P}_g] + g_{BG} \cdot \mathcal{P}_{BG}, \tag{2}$$

where g_{BG} is the fraction of the background candidates in the D^* sample. The variables g_b, g_c and g_g are, respectively, the fractions of D^* mesons produced from a primary b quark, c quark, and a gluon splitting into a pair of heavy quarks. By construction, these fractions satisfy the relation $g_b + g_c + g_g = 1$. The parameters $\mathcal{P}_c$, $\mathcal{P}_b$ and $\mathcal{P}_g$ describe the probability that a D^* from one of these classes will be tagged by the bottom-tagging methods, and $\mathcal{P}_{BG}$ is the probability that a background D^* candidate is tagged.

The tagging techniques distinguish between two classes of events, b-like and not b-like. The previous equation can be rewritten in terms of only two components by dividing the contribution from gluon splitting, $g_g \cdot \mathcal{P}_g$, into $\alpha \cdot g_g \cdot \mathcal{P}_b$ and $(1 - \alpha) \cdot g_g \cdot \mathcal{P}_c$, where

$$\alpha \equiv \frac{\mathcal{P}_g - \mathcal{P}_c}{\mathcal{P}_b - \mathcal{P}_c} \ . \tag{3}$$

With this definition, the parameter α describes the effective fraction of gluon splitting events that are assigned to the b-sample as a result of the separation techniques. Defining effective fractions f_b and f_c as

$$f_b = g_b + \alpha \cdot g_g \quad \text{and} \quad f_c = g_c + (1 - \alpha) \cdot g_g \ , \tag{4}$$

with $f_b + f_c = 1$, equation 2 can be rewritten as

$$\frac{N_{b-tag}}{N_{cand}} = (1 - g_{BG}) \cdot [f_b \cdot \mathcal{P}_b + (1 - f_b) \cdot \mathcal{P}_c] + g_{BG} \cdot \mathcal{P}_{BG} \ . \tag{5}$$

From this f_b, the effective fraction of b-like events in the sample, is determined under the assumption, that $\mathcal{P}_b$, $\mathcal{P}_c$, $\mathcal{P}_{BG}$ and g_{BG} are known. To determine the fragmentation function this calculation is done for a series of bins in x_{D^*}.

5.1 High momentum leptons

Leptons with high p and p_t are a well established signature for b decays. Here p_t is the lepton momentum component transverse to the jet which contains it. We search for leptons in D^* candidate events as a method to tag b decays. Leptons found in the thrust hemisphere containing the D^* (designated $D^*\ell$), and in the hemisphere not containing the D^* (designated D^*/ℓ) are used. A b-enriched sample of events is prepared by requiring

- $p^e > 2.0$ GeV/c and $p_t^e > 0.8$ GeV/c for electrons, and

- $p^\mu > 3.0$ GeV/c and $p_t^\mu > 0.8$ GeV/c for muons.

The methods used to identify the leptons are described in detail in [17, 18]. Background in the sample is reduced by allowing only certain charge combinations to be used:

- $\mathrm{D}^{*+}\ell^-$ for events with D^* and ℓ in the same hemisphere;
- $\mathrm{D}^{*+}\ell^+$ for events with D^* and ℓ in opposite hemispheres.

In the second case the charge correlation is diluted due to $\mathrm{B}^0\bar{\mathrm{B}}^0$ mixing. Most D^* mesons are produced in decays of B^0_d mesons. This has been demonstrated to be a reasonable assumption at least in semileptonic decays, where only $16^{+16}_{-10}\%$ [19, 20] are found to come from B^+ mesons. To determine the mixing parameter in the D^* hemisphere, $\chi_{\mathrm{D}^*_{hem}} = 0.84 \cdot \chi_\mathrm{d}$, we use the world average value for $x_\mathrm{d} = \Delta m_{\mathrm{B}^0_\mathrm{d}}/\Gamma_{\mathrm{B}^0_\mathrm{d}} = 0.71 \pm 0.06$ [1] and convert this into a value for the average mixing parameter $\chi_\mathrm{d} = 0.168 \pm 0.019$. In the other hemisphere we use the average B mixing as determined by OPAL, since all types of B mesons contribute: $\chi = 0.143^{+0.022}_{-0.021} \pm 0.007$ [22]. Thus the total probability that mixing has occurred and destroyed the charge correlation is given by:

$$\chi_{\mathrm{D}^*/\ell} = \chi_{\mathrm{D}^*_{hem}} \cdot (1-\chi) + \chi \cdot (1 - \chi_{\mathrm{D}^*_{hem}}) = 0.244^{+0.031}_{-0.028} \ ,$$

where the error quoted contains both the statistical and systematic errors.

The level of background in the sample is estimated by using the different D^* background samples discussed above, combined with all possible charge combinations of the lepton candidate. Monte Carlo studies show that fake D^* mesons are the dominant background source, justifying this method. We subtract the background after normalising it to the D^* lepton sample in a sideband of $160 < \Delta M < 200$ MeV/c^2. After background subtraction we find 105 ± 13 $\mathrm{D}^*\ell$ candidates, and 61 ± 13 D^*/ℓ candidates, over backgrounds of 27 ± 5 and 40 ± 6 events respectively. Most of the background is concentrated in the region $x_{\mathrm{D}^*} < 0.2$, with 20 (22) background events found in this region alone.

The efficiency for finding a lepton in either hemisphere, including the semileptonic branching ratios, is determined from Monte Carlo to be

$$\varepsilon_{\mathrm{D}^*\ell} = (8.9 \pm 0.4)\% \qquad \varepsilon_{\mathrm{D}^*/\ell} = (7.6 \pm 0.4)\%.$$

Monte Carlo studies have shown that apart from the small difference in overall efficiency no significant bias is introduced for the x_{D^*} distribution for events where the D^* and the lepton are identified in the same jet. In Figure 2 we show the ΔM distributions for $\mathrm{D}^*\ell$ and D^*/ℓ candidates, with the background distributions superimposed.

5.2 Jet shape variables

Due to the high b mass and the hard b fragmentation, the shapes of b jets are expected to be significantly different from those of u, d, s or c jets. This is used to construct a separation procedure based on a number of jet shape variables. To eliminate the bias caused by the presence of a D^* meson in a jet, only jets not containing a D^* candidate are used. We maximise the probability of tagging a quark, rather than a gluon jet, by using the most energetic jet which does not contain the D^* .

Seven jet shape variables are calculated for this jet. A detailed description and discussion may be found in the appendix A. The variables are constructed to exploit the differences in mass and average energy between bottom and light quarks. Since the differences in the distributions

of these variables for $b\bar{b}$ and light quark events are small and highly correlated, we use an artificial neural network (ANN) [23] to separate the two event classes. A similar technique has been used in Reference [24].

The interpretation of the output of the network relies crucially on the understanding of the training and test samples used. We use a $b\bar{b}$-enriched selection of events from the data, and $c\bar{c}$ Monte Carlo events to train the network. In each case the samples are divided into two equally sized subsamples – one to train the network and the other to calculate the tagging efficiencies of the trained network. We select the $b\bar{b}$ events for training using identified leptons with high p and p_t. A purity of 92.0% is achieved [17, 18] by requiring:

- $p^{\mathrm{e}} > 2.0$ GeV/c and $p_t^{\mathrm{e}} > 1.3$ GeV/c for electrons, and
- $p^{\mu} > 3.0$ GeV/c and $p_t^{\mu} > 1.5$ GeV/c for muons,

where p_t is calculated with respect to the axis of the jet containing the lepton. The jet shape variables in the training sample are formed for the most energetic jet which does not contain the lepton. The $c\bar{c}$ training sample is generated using the JETSET7.3 Monte Carlo followed by the OPAL detector simulation. In the data the procedure of selecting those jets to calculate the jet shape variables which do not contain the D^* and have the next highest energy, creates a mixture of highest- and second-highest energy jets. This mixture is reproduced in the training sample by appropriately selecting jets.

We divide the data into four samples of roughly equivalent size, characterised by the output of the ANN, from b-depleted to b-enriched. We determine the background in the samples from the wrong charge D^* events. We do not use the reflected pion background, in order not to distort the jet shape variable distributions by changing the jet multiplicity. We normalise this background sample to the number of expected background events as measured in section 4.2 and given in table 1, and subtract it from the candidate sample. The fraction of b events is determined using equation 5.

In Figure 3 the jet shape variables for the combined training and test samples are shown separately for $b\bar{b}$ and $c\bar{c}$ events. The corresponding distributions for the D^* candidates are superimposed. The $b\bar{b}$ and $c\bar{c}$ events are weighted according to their normalisation measured with the ANN. Figure 4 shows a similar distribution for the output of the ANN. Reasonable agreement between data and Monte Carlo is seen. Possible differences are addressed as a systematic error.

5.3 Separating b/c with Lifetime Information

The measurably long lifetimes of heavy hadrons, in particular those containing a b quark, can be used to separate events according to their flavour. Since heavy hadrons are produced in pairs, normally both hemispheres in an event contain this information[4]. We take advantage of this and use two separation techniques in the two hemispheres.

In the hemisphere opposite the D^* candidate, no attempt is made to reconstruct exclusively the heavy hadron or its decay products. Instead we calculate the forward multiplicity [25], essentially the number of tracks significantly separated from the primary vertex. For each track an impact parameter is calculated in the r-ϕ plane, defined as the distance of closest approach of the track to the primary vertex of the event. The axis of the jet containing the track in question is used to determine the sign of the impact parameter. The sign is set positive if

[4]The hemispheres are defined using the thrust direction as discussed in Section 3.

the track crosses the jet axis in the same hemisphere in which the track is found, where the hemisphere is defined by the primary vertex and the thrust direction.

The number of tracks which are separated from the primary vertex by more than 2.5 times the combined track impact parameter and beam size errors is used as the flavour separation variable. An event is called tagged, if more than 2 tracks fullfill this condition. Contributions from other long lived particles are reduced by including only tracks with an absolute impact parameter of less than 3 mm. Tracks with an error larger than 1 mm are rejected.

To improve the resolution in the impact parameter we use only tracks from data collected in 1991 and 1992, after the silicon microvertex detector [7] became operational. However, no requirement is made on individual tracks to have silicon hits. The distribution of the forward multiplicity in the hemispheres opposite to the D^* candidates is compared to the Monte Carlo prediction in Figure 5. The tagging efficiencies for b and c events are calculated from Monte Carlo events. Within the available statistics no correlation of efficiencies with x_{D^*} is found. We therefore calculate global efficiencies for $b\bar{b}$ and for $c\bar{c}$ events. The forward multiplicity distribution of the background is measured using events tagged as background with the methods described in Section 4.2, and subtracted from the sample.

The probability values found are $\mathcal{P}_{BG} = 0.280 \pm 0.006$, $\mathcal{P}_{\rm b} = 0.550 \pm 0.010$ and $\mathcal{P}_{\rm c} = 0.201 \pm 0.007$, where these errors are statistical only. The fractions of b-events are calculated using equation 5.

In the second technique based upon lifetime information we reconstruct the distance between the primary event vertex and the decay vertex of the D^0 candidate. A similar technique has been used in Reference [26]. For b decays the measured distance is a convolution of that resulting from the B meson, and that from the D^0. In c decays, only the D^0 lifetime contributes. We analyse each x_{D^*} bin separately since a strong correlation exists between the measured decay length and the energy of the D^*.

The D^0 decay vertex is determined by finding the intersection of the two candidate D^0 tracks in the r-ϕ plane. The decay length, d, of this candidate vertex is calculated by taking the distance between this vertex and the primary event vertex, constrained by the direction of the jet containing the D^* candidate. We separate b from c events by using the decay length significance $D = d/\sigma_d$, where σ_d is the error of the decay length. In Figure 6 the observed decay length significance distribution is shown. The same distribution from Monte Carlo is superimposed.

We determine the background in this distribution from data, by using the D^* background samples discussed in section 4.2. Monte Carlo studies have shown that all three background samples model the decay length significance distribution of the true D^* background very well. In a given x_{D^*} bin we take the decay length significance distribution of the background sample and normalise it to the total number of background events expected in this x_{D^*} bin. This normalised distribution is subtracted bin by bin from the candidate distribution, giving the distribution of true D^* mesons.

The Monte Carlo is used to calculate the probability for tagging a bottom decay for a given cut, in a particular x_{D^*} bin, and to calculate the contamination from charm events. The fraction of b events in this x_{D^*} bin can then be calculated using equation 5. We repeat the analysis for four different cuts in decay length significance, cutting at $D = 4, 6, 8$ and 10. The results are combined taking into account the correlations between the samples.

5.4 Systematic errors

A number of effects result in systematic errors on the fraction $f_{\rm b}$ in each of the analyses. In this section we first discuss those errors correlated between at least two analyses, followed by a description of the uncorrelated ones.

The following errors are shared by all four techniques:

- Background determination: In all four cases the background is determined using the different background samples constructed in data and discussed above. The error assigned is found by comparing the results extracted from these different samples with each other, and by comparing the background samples with Monte Carlo samples.

- Background flavour composition: An incorrect flavour composition of the background samples compared to the true background can significantly distort the tagging efficiencies. We study these effects in Monte Carlo events.

- Monte Carlo statistics: All analyses use Monte Carlo events to calculate at least some of the tagging efficiencies. Since a large but finite Monte Carlo sample is used, we assign an error from this source to each analysis.

- b/c fragmentation: For most analyses, the calculation of tagging efficiencies depends to some extent on the fragmentation of b and c quarks used in the Monte Carlo. We change the fragmentation parameters for both b and c fragmentation functions, assuming a Peterson shape, within their measured values: $0.0038 < \epsilon_b < 0.0085$ [22], and $0.03 < \epsilon_{\rm c} < 0.07$ [4, 27] respectively. The effects from this for the final analysis are small. The jet shape analysis is not sensitive to the b fragmentation in the Monte Carlo, since data are used to train the net for b recognition.

The following errors are shared only between two analyses.

- Lepton identification: Both the $\mathrm{D}^*\ell$ and the jet shapes analyses use leptons to tag b decays. We investigate the influence of the semileptonic decay branching ratio and lepton identification probabilities [22] by varying them within their errors. We reweight the lepton p and p_t spectra with different models [28], as discussed in [22].

- B hadron lifetimes: The lifetime analyses are sensitive to the lifetimes of the b and c hadrons used in the Monte Carlo. The charmed hadron lifetimes are well measured, with small errors compared to the bottom hadron ones. We vary them within their experimental errors [1] and find minimal dependence. More importantly we vary the bottom hadron lifetimes. Tags using the hemisphere opposite to the D^* are sensitive to the mixture of B hadrons at LEP, for which the lifetime has been measured precisely: 1.537 ± 0.021 ps [1]. Those tags using the hemisphere containing the D^* are mostly sensitive to the lifetime of neutral B mesons. In order to be consistent with current measurements [1] we assume equal lifetimes for neutral and charged B mesons, but assign a 10% error to this [29].

- Detector resolution: The lifetime analyses are sensitive to the resolution of the decay length reconstruction. We investigate effects of the detector resolution by varying the additional smearing added to d_0 and ϕ_0 from an optimal value of 1.4 by ± 0.2 (see Section 3). Also important for both analyses is the knowledge of the primary beam spot. We change both position and width by ± 1 standard deviation, corresponding to a change of the nominal beam position by $25\,\mu$m, and the assumed width by $\pm 10\mu$m.

The following errors are unique for individual analyses:

- Monte Carlo modelling of charm decays: In the jet shape analysis we use the Monte Carlo to model the $c\bar{c}$ events used to train the network. Possible modelling problems are investigated by comparing a sample of multihadronic Monte Carlo events to an unbiased data sample. We compare the network output distributions of both samples and find the differences to be small. Under the assumption that all observed differences are due to the $c\bar{c}$ events we derive a set of correction factors for the network output distribution, which we translate into a variation of the corresponding identification probabilities. This error is the largest single systematic error in the jet shape analysis, reaching about half the size of the statistical error.

- Detector response in $\cos\theta$: The detector response is different for central and for endcap events. The jet shape analysis is sensitive to this, since the events used to train the network are different from those to which it is eventually applied. If the $\cos\theta$ distribution of the test and the candidate samples are different, a systematic errors arise. We estimate this by training the net separately for central and endcap events, comparing these results to those obtained by training the network on the combined sample, and assigning the difference as the systematic error.

- Potential bias between the jet and the D^* : The jet shape analysis relies on the assumption that the jet investigated is unbiased by the presence of a D^* in the event. However, due to phase space effects a small correlation between both jets is expected. A Monte Carlo sample with 17000 D^* events is divided into events with candidates with $x_{D^*} > 0.5$ and $x_{D^*} < 0.5$. For both subsamples the identification probabilities are calculated. The differences between these lead to differences in the b-fractions that are included as a systematic error.

- $B^0\bar{B}^0$ mixing: In the D^* lepton analysis we need to correct the opposite side D^* lepton sample for mixing in the neutral B sector. We use the errors quoted above for the effective mixing to estimate its influence.

- B multiplicity: The analysis using forward multiplicity in the opposite hemisphere is sensitive to the B decay multiplicity in the Monte Carlo. This multiplicity has been measured in multihadronic Z^0 decays to be 5.5 ± 0.5 [30] and is allowed to vary within its experimental error.

5.5 Combined analysis

We combine the results from the four analyses by minimising the χ^2

$$\chi^2 = \Delta\vec{A}^T \cdot \mathcal{C}^{-1} \cdot \Delta\vec{A} \ , \tag{6}$$

where $\Delta\vec{A}$ is the vector

$$\Delta\vec{A} = (f_{b,(1)} - f_b \ , \ f_{b,(2)} - f_b \ , \ f_{b,(3)} - f_b \ , \ f_{b,(4)} - f_b) \ , \tag{7}$$

and f_b is the fraction of D^* mesons from b -like decays for the combined result. The parameter $f_{b,(i)}$ is the measured fraction in analysis i, and $\mathcal{C}$ the covariance matrix. The latter is defined

as

$$\begin{aligned} \mathcal{C}_{ii} &= (\sigma_i^{\rm stat})^2 + \sum_{n=1}^{N} (\sigma_{i,n}^{\rm sys})^2 \\ \mathcal{C}_{ij} &= \sum_{n=1}^{N} p_{ij,n} \cdot \sigma_{i,n}^{\rm sys} \cdot \sigma_{j,n}^{\rm sys} \quad i \neq j \ , \end{aligned} \tag{8}$$

where the indices i, j run over the four analyses combined, and n over the different systematic errors as listed in the previous sections. The factor $p_{ij,n}$ describes the correlation between errors i and j for error n. We have assumed $p_{ij} = +1$ for all correlated errors. This combination is possible because the four methods are largely statistically uncorrelated, with each separation method relying on different observables in the event. Correlations in the systematic errors between the different $x_{\rm D^*}$ bins have been investigated and are found to have a negligible effect on the resulting combination.

The final results for the ratios $f_{\rm b}$ and $f_{\rm c}$ are given in Table 2. Also shown are the statistical errors, and the different systematic errors as discussed in the previous section. The ratio $f_{\rm b}$ is plotted in Figure 7, together with the results of the individual analyses. Good agreement between all four methods is observed. The χ^2 for the fit for all 10 ratios including systematic errors is 24.9 for 30 degrees of freedom.

In Table 3 and Figure 8 the differential yield of $\rm D^*$ mesons as a function of $x_{\rm D^*}$ is shown separately for $\rm b\bar{b}$ and $\rm c\bar{c}$ events.

6 Results

In this section, we use the full and the flavour separated $\rm D^*$ event samples to calculate the total production rate of $\rm D^*$ mesons in multihadronic events, and to investigate the properties of the production of $\rm D^*$ mesons in c and b decays.

6.1 Inclusive yield

From the results presented in Table 1 we determine the total yield of charged $\rm D^*$ mesons via the decay channel $\rm D^* \to D^0\pi$, $\rm D^0 \to K\pi$. Since we measure $\rm D^*$ production from close to the production threshold at $x_{\rm D^*} \approx 0.04$ to $x_{\rm D^*} = 1$, we can simply calculate this from the total number of $\rm D^*$ mesons observed as given in table 1 and the efficiencies. We find

$$\bar{n}_{\rm Z^0 \to D^* X} \cdot B(\rm D^* \to D^0\pi) \cdot B(D^0 \to K\pi) \;=\; (5.01 \pm 0.25 \pm 0.20) \cdot 10^{-3} \ ,$$

where $\bar{n}_{\rm Z^0 \to D^* X}$ is the total inclusive yield of the sum of positively and negatively charged $\rm D^*$ mesons per hadronic $\rm Z^0$ decay. The first error quoted is the statistical error and the second the systematic error. The dominant contributions to the systematic errors are from detector effects as discussed above.

Dividing by the branching ratios $B(\rm D^* \to D^0\pi) = 0.681 \pm 0.013$ and $B(\rm D^0 \to K\pi) = 0.0401 \pm 0.0014$ [1] we find

$$\bar{n}_{\rm Z^0 \to D^* X} = 0.183 \pm 0.009 \pm 0.007 \pm 0.008 \ ,$$

where the first error quoted is the statistical error, the second one is the systematic error, and the third is the error due to the $\rm D^*$ and $\rm D^0$ branching ratios used.

x_{D^*}	$0.0-0.1$	$0.1-0.2$	$0.2-0.3$	$0.3-0.4$	$0.4-0.5$	$0.5-0.6$	$0.6-0.7$	$0.7-0.8$	$0.8-0.9$	$0.9-1.0$
f_b	0.64	0.38	0.705	0.796	0.623	0.316	0.143	0.005	0.058	0.34
statistical error	0.50	0.10	0.053	0.056	0.055	0.053	0.052	0.047	0.080	0.26
systematic error	0.30	0.10	0.056	0.053	0.045	0.039	0.043	0.049	0.044	0.059
	individual systematic errors									
background	0.20	0.051	0.023	0.015	0.013	0.011	0.019	0.029	0.009	0.013
background flavour	0.10	0.031	0.035	0.023	0.014	0.013	0.006	0.003	0.004	0.013
Monte Carlo stat.	0.07	0.023	0.013	0.014	0.015	0.012	0.010	0.010	0.018	0.019
b/c fragmentation	0.05	0.017	0.006	0.008	0.006	0.005	0.003	0.003	0.004	0.013
lepton ID, purity	0.02	0.007	0.009	0.010	0.010	0.007	0.005	0.003	0.008	0.013
τ_B, τ_D	0.07	0.022	0.013	0.015	0.020	0.020	0.020	0.020	0.025	0.027
detector resolution	0.07	0.023	0.014	0.016	0.020	0.020	0.021	0.020	0.026	0.027
charm modelling	0.03	0.010	0.011	0.019	0.014	0.009	0.009	0.009	0.014	0.017
$\cos\theta$, hem. bias	0.05	0.016	0.017	0.017	0.003	0.008	0.003	0.004	0.004	0.004
$B^0\overline{B}^0$ mixing	0.02	0.006	< 0.001	0.003	< 0.001	0.002	< 0.001	< 0.001	0.003	0.013
B multiplicity	0.03	0.020	0.021	0.026	0.017	0.010	0.020	0.023	0.015	0.020

Table 2: Fraction of D^* events from b decays, f_b, along with the statistical and the systematic errors. Since $f_c = 1 - f_b$ the errors on f_c are the same as those on f_b. The different systematic errors are discussed in detail in the text.

x_{D^*}	$(1000/N_Z)\cdot(dN_{b\to D^*}/dx_{D^*})$	$(1000/N_Z)\cdot(dN_{c\to D^*}/dx_{D^*})$
0.0-0.1	$0.44 \pm 1.08 \pm 1.09$	$0.26 \pm 0.70 \pm 0.65$
0.1-0.2	$2.80 \pm 0.91 \pm 0.78$	$4.49 \pm 1.11 \pm 0.86$
0.2-0.3	$7.68 \pm 0.82 \pm 0.79$	$3.22 \pm 0.63 \pm 0.64$
0.3-0.4	$7.26 \pm 0.72 \pm 0.60$	$1.86 \pm 0.53 \pm 0.49$
0.4-0.5	$4.82 \pm 0.54 \pm 0.40$	$2.92 \pm 0.47 \pm 0.37$
0.5-0.6	$1.89 \pm 0.34 \pm 0.25$	$4.10 \pm 0.42 \pm 0.28$
0.6-0.7	$0.59 \pm 0.22 \pm 0.18$	$3.50 \pm 0.34 \pm 0.21$
0.7-0.8	$0.02 \pm 0.14 \pm 0.15$	$3.02 \pm 0.31 \pm 0.18$
0.8-0.9	$0.07 \pm 0.10 \pm 0.05$	$1.12 \pm 0.19 \pm 0.06$
0.9-1.0	$0.03 \pm 0.03 \pm 0.01$	$0.07 \pm 0.04 \pm 0.01$

Table 3: Differential yields for D^* mesons in $b\bar{b}$ and $c\bar{c}$ decays, normalised to the total number of multihadronic Z^0 decays, N_Z, as reconstructed using all four separation methods. The errors quoted are the statistical and the total systematic error, containing contributions from the separation methods, and from the total yield of D^* mesons.

6.2 Flavour-dependent studies

We use the flavour separated D^* samples discussed in Section 5 to study the production of charmed mesons in multihadronic decays of the Z^0. There are three main sources of charmed mesons in Z^0 decays: primary b events, primary c events, and gluons splitting into a pair of heavy quarks.

The least well investigated of these three processes is the splitting of gluons into heavy quarks. Improved calculations for the rate of gluon splitting in e^+e^- collisions have recently become available, using next to leading order logarithmic resummation techniques combined with the exact result to leading order [31]. In Table 4 results from calculations and Monte Carlo models for the multiplicity of the process $g \to c\bar{c}$ and $g \to b\bar{b}$ are summarised. The multiplicities, $\bar{n}_{g\to c\bar{c}}$ and $\bar{n}_{g\to b\bar{b}}$, are defined as the number of $c\bar{c}$ ($b\bar{b}$) pairs from gluon decay, in the process $g \to c\bar{c}$ ($b\bar{b}$), divided by the total number of hadronic Z^0 decays. Although different models differ significantly, all agree in the prediction that these processes are considerably suppressed due to the large mass scale at which the gluon needs to be created. The models also predict that the rate for gluon splitting into heavy quark pairs is independent of the flavour of the quark into which the Z^0 decayed, to the level of about 10%.

The flavour separation technique described in the previous section divides the D^* sample into two fractions on a statistical basis, a c-like and a b-like one. The third component contributing to the signal, that from gluon splitting, is distributed between these two. From a study of a Monte Carlo sample produced using JETSET, we find that a fraction[5] $\alpha = 0.145 \pm 0.075$ of all D^* mesons from gluon splitting events are attributed to the b-like sample. We have assigned a 50% error to this number to account for possible modelling problems in the Monte Carlo.

We determine the total yields of D^* mesons in the three different production channels by a combination of fitting and counting techniques. Since most D^* mesons produced from gluon splitting are detected in the c-like sample, the rates of D^* mesons from $g \to Q\bar{Q}$ (where Q=c,b) and from primary charm are determined in a fit to the c-like sample. We use the JETSET

[5]The parameter α was defined in equation 3.

Method	$\bar{n}_{g\to c\bar{c}}$ (%)	$\bar{n}_{g\to b\bar{b}}$ (%)	r_{gb}
Resummed + leading order	1.35	0.177	0.116
Leading order	0.607	0.100	—
HERWIG [52]	0.923±0.005	0.227±0.001	0.197
JETSET [13]	1.701±0.013	0.160±0.004	0.086
ARIADNE [35]	2.177±0.015	0.326±0.006	0.130
average			0.132 ± 0.047

Table 4: The multiplicity of $c\bar{c}$, $b\bar{b}$ pairs in Z^0 decays due to gluon splitting ($\bar{n}_{g\to c\bar{c}}$, $\bar{n}_{g\to b\bar{b}}$) as predicted in different calculations and models. The errors shown are purely due to Monte Carlo statistics (from Reference [31]). In the last column the ratio $r_{gb} = \bar{n}_{g\to b\bar{b}}/(\bar{n}_{g\to c\bar{c}} + \bar{n}_{g\to b\bar{b}})$ is given, together with the average. The second value is not included in the average since it is included in the first. The error quoted is the standard deviation of the five values.

model to predict the shape of both the $Z^0 \to c\bar{c} \to D^*$ and the $g \to Q\bar{Q} \to D^*$ components. For brevity, these components will hereafter be referred to as "$c \to D^*$" and "$g \to D^*$", respectively. The shape of the fragmentation function is described by a Peterson function [15] formulated in the variable $z = (E + p_\parallel)_{\rm hadron}/(E + p_\parallel)_{\rm quark}$, with the momenta measured relative to the direction of the string in the model. The parameter of the fragmentation function is forced to be the same for the $c \to D^*$ and $g \to D^*$ processes. Since z is not experimentally accessible, the JETSET Monte Carlo is used to do the conversion from the distribution in z to one in x_{D^*}. For the shape of the gluon component we use a mixture of $g \to c\bar{c} \to D^*$ and $g \to b\bar{b} \to D^*$ events as predicted by JETSET, with a relative ratio given by the average in Table 4.

Using the definitions

$$\begin{aligned} F_{q\bar{q}} &\equiv \Gamma(Z^0 \to q\bar{q})/\Gamma(Z^0 \to \text{hadrons}) & (9)\\ P_q &\equiv B(q \to D^*) \cdot B(D^* \to D^0\pi) \cdot B(D^0 \to K\pi) & (10)\end{aligned}$$

for a quark of flavour q, we describe the observed spectrum $(1/N_{\rm had}dN/dx)_c$ in c-like events by:

$$R_c(x_{D^*}) = 2 \cdot \{F_{c\bar{c}} \cdot P_c \cdot f_c(x_{D^*}, \langle x_{c\to D^*}\rangle) + (1-\alpha) \cdot F_{g\to Q\bar{Q}} \cdot P_g \cdot f_g(x_{D^*})\}, \quad (11)$$

where f_c and f_g are the normalised fragmentation functions for $c \to D^*$ and $g \to D^*$, respectively, $F_{g\to Q\bar{Q}}$ is the fraction of Z^0 decays where a gluon splits into a pair of heavy quarks Q, P_g is defined as in equation 10, but for quarks produced from gluon splitting, and $\alpha = 0.145 \pm 0.075$ has been defined above. We have assumed that threshold effects very close to the kinematic limit of D^* production do not play a significant role, allowing us to define P_c, P_g as independent of x_{D^*}. We find

$$\begin{aligned} F_{c\bar{c}} \cdot P_c &= (1.006 \pm 0.055 \pm 0.061) \cdot 10^{-3}\\ \langle x_{c\to D^*}\rangle &= 0.515^{+0.008}_{-0.005} \pm 0.010\\ F_{g\to Q\bar{Q}} \cdot P_g &= (0.30 \pm 0.10 \pm 0.10) \cdot 10^{-3}\ , & (12)\end{aligned}$$

where both the statistical and systematic error (described in detail below) are given. The χ^2 of the fit is 7.0 for 7 degrees of freedom. The correlation coefficients including systematic errors are listed in Table 5. The results are illustrated in Figure 9, where the yield from c-like

Parameter	$F_{c\bar{c}} \cdot P_c$	$\langle x_{c\to D^*} \rangle$	$F_{g\to Q\bar{Q}} \cdot P_g$
$F_{c\bar{c}} \cdot P_c$	1.00	0.26	-0.23
$\langle x_{c\to D^*} \rangle$		1.00	0.14
$\bar{n}_{g\to D^* X}$			1.00

Table 5: Correlation coefficients for the fit to the $c \to D^*$ spectrum, including statistical and systematic errors.

Systematic error	$F_{c\bar{c}} \cdot P_c$	$\langle x_{c\to D^*} \rangle$	$F_{g\to Q\bar{Q}} \cdot P_g$	$F_{c\bar{c}}$
D^* reconstruction	0.015	0.002	0.05	0.002
b/c separation	0.027	0.005	0.08	0.004
fragmentation model	0.046	0.008	0.03	0.007
$g \to c\bar{c}$ model	0.025	0.004	0.01	0.004
$g \to c\bar{c}$ in b sample			0.03	
Total systematic error	0.061	0.010	0.10	0.009

Table 6: Systematic errors from the fit to the x_{D^*} distribution of the c-like sample. The entry 'D^* reconstruction' corresponds to the systematic error due to the D^* efficiency and background determination of sections 4.2 and 4.3. The entry 'b/c separation' refers to the systematic errors related to the determination of f_b (see Table 2).

events is shown as a function of x_{D^*}, with the result from the fit for the different components superimposed.

Similarly the total yield of D^* mesons in b-like events is described by

$$R_b(x_{D^*}) = 2 \cdot \{F_{b\bar{b}} \cdot P_b \cdot f_b(x_{D^*}, \langle x_{D^*} \rangle) + \alpha \cdot F_{g\to Q\bar{Q}} \cdot P_g \cdot f_g(x_{D^*})\} \ . \tag{13}$$

To be independent of any specific B-hadron decay model used we do not assume any shape for the $b \to D^*$ fragmentation function, but simply sum the x-dependent yields given in Table 3 for the b-like sample. We use the results for $F_{g\to Q\bar{Q}} \cdot P_g$ from the fit to the c-like sample and obtain:

$$F_{b\bar{b}} \cdot P_b \quad = \quad (1.24 \pm 0.10 \pm 0.09) \cdot 10^{-3} \ . \tag{14}$$

The error is larger than the error on the D^* yield in charm events, because no particular fragmenation model has been assumed for the calculation.

It should be pointed out that contrary to other analyses [24, 26], we quote a number for $\langle x_{c\to D^*} \rangle$ and for both the b and the c yield without any contribution from $g \to D^*$. In particular our number for $\langle x_{c\to D^*} \rangle$ cannot be directly compared to numbers quoted in these references. Monte Carlo studies indicate that the difference in the treatment of the gluon component may shift $\langle x_{D^*} \rangle$ by as much as 0.015, increasing the values quoted in [24, 26], when only primary $c \to D^*$ decays are considered.

The systematic errors, which are listed in Table 6, include the effects of errors from the b/c separation procedures, errors in the D^* reconstruction, and additional errors which are caused by the above fit having to assume specific functional forms for the $c \to D^*$ fragmentation function and for the $g \to c\bar{c}$ spectrum. In particular the errors considered are the following:

- We have repeated the analysis with four different models for the shape of the $c \to D^*$ fragmentation function: Peterson [15], Collins and Spiller [32], Lund symmetric [33], and Kartvelishvili [34] (for a more detailed description of these models see Section 6.3). The uncertainty due to fragmentation modelling is estimated as the standard deviation of the results obtained with the different models.

  For the mean scaled energy, $\langle x_{c \to D^*} \rangle$, we have checked this error by determining the weighted average in the region $x_{D^*} > 0.2$, where there is much less sensitivity to gluon splitting, according to

$$\langle x_{c \to D^*} \rangle = \frac{\sum N_{D^*,i} \cdot f_{c,i} \cdot x_i}{\sum N_{D^*,i} \cdot f_{c,i}} \qquad (\text{for } x_{D^*} > 0.2), \tag{15}$$

  where $N_{D^*,i}$ is the number of candidates in bin i of x_{D^*}, as given in Table 1 and $f_{c,i}$ is the fraction of D^* from c decays in that bin (see Table 2). We find $\langle x_{c \to D^*} \rangle = 0.542 \pm 0.016 \pm 0.015$. This result agrees well with that determined with the fit, where we find a mean scaled energy of $0.547 \pm 0.008 \pm 0.008$ for $x_{D^*} > 0.2$.

  A similar check is performed for the yield, $F_{c\bar{c}} \cdot P_c$, for $x_{D^*} > 0.2$. In this case, we have recalculated the yield simply by summing the bins in this range of x_{D^*}, after subtracting the measured component from gluon splitting. This is compared to the result of repeating the fit (with a gluon splitting contribution fixed to the result found with the nominal fit) over this same range. We find from the fit a value of $F_{c\bar{c}} \cdot P_c = (0.94 \pm 0.07) \cdot 10^{-3}$, and from counting $F_{c\bar{c}} \cdot P_c = (0.91 \pm 0.08) \cdot 10^{-3}$ for $x_{D^*} > 0.2$, in very good agreement.

- We used the Monte Carlo models ARIADNE [35] and JETSET to investigate the dependence on the shape of the $g \to c\bar{c}$ spectrum. The difference between the fit results when these two models are used is taken as the systematic error.

- The result for the gluon yield is sensitive to the leakage α of $g \to D^*$ candidates into the b-like sample. The correction for this leakage is based on a Monte Carlo simulation. The error assigned is 50% of the correction and includes both a statistical error due to the finite size of the Monte Carlo sample used, and a systematic error from uncertainties in the modelling of $g \to c\bar{c}$ in the Monte Carlo.

6.2.1 The Partial Width $\Gamma_{c\bar{c}}/\Gamma_{had}$

We convert the production rate for D^* mesons from primary $c\bar{c}$ into the partial width, $\Gamma_{c\bar{c}}/\Gamma_{had}$, by dividing by the product branching ratio P_c. No published measurement of the latter quantity exists for LEP energies. We therefore use an average of measurements at energies of 10.5 GeV [36] and around 30 GeV [37, 38, 39], similar to the procedure followed in Reference [4]. The experiments at these lower energies quote directly the product branching ratio P_c, making the calculation independent of the value and error of the individual branching ratios $B(D^* \to D^0\pi)$ and $B(D^0 \to K\pi)$. The validity of this procedure depends on the assumption that the sources of D^* mesons in charm decays are the same at LEP energies as they are at lower energies. This assumption is supported by Monte Carlo studies and is consistent with the measured D^* yields at energies around 10 and 30 GeV. A possible source for a difference could be a change in the relative production of D^* mesons from excited D states. However, the assumption that no significant differences exist is supported by experiment, where for instance, the fraction of the D^* sample due to $D^{**} \to D^*X$ decays has been measured to be $21 \pm 8\%$ at

10 GeV [40] and $18 \pm 5\%$ at Z^0 energies [24]. We obtain $P_c = (7.1 \pm 0.5) \cdot 10^{-3}$, where the error quoted contains the statistical and systematic error of the measurement. This yields:

$$\frac{\Gamma(Z^0 \to c\bar{c})}{\Gamma(Z^0 \to \text{hadrons})} = 0.142 \pm 0.008 \pm 0.009 \pm 0.011 \ .$$

The errors quoted are the statistical error, the systematic error from this analysis, and a systematic error due to the uncertainty in the branching ratios used to extract the result. This result is 1.7 standard deviations below the expectation in the Standard Model of $F_{c\bar{c}} = 0.171$ [41] with the largest uncertainty from the use of lower energy measurements.

Alternatively we calculate the relative production rate of D^* events in c decays to that in b decays, using predictions in the Standard Model for $F_{b\bar{b}} = 0.216$ and $F_{c\bar{c}} = 0.171$[6] [41]. We find

$$\frac{B(c \to D^*)}{B(b \to D^*)} = 1.03 \pm 0.11 \pm 0.10 \ ,$$

which can be compared to $B(c \to D^*)/B(b \to D^*) = 1.36 \pm 0.20$ as derived from published values for the individual branching ratios[7]. Good agreement is observed with recent LEP measurements [24, 26].

6.2.2 Gluon splitting

The differential yield of D^* mesons in the c-tagged sample is shown in Figure 9(b), together with the component from primary quark production and from gluon splitting. In Figure 9(a) the χ^2 contour for the fit in the $\langle x_{c \to D^*} \rangle$ versus $F_{g \to Q\bar{Q}} \cdot P_g$ plane is displayed. If we repeat the fit with the gluon component set to zero, the χ^2 increases from 7.0 for 7 degrees of freedom to 11.2 for 8 degrees of freedom (including the systematic errors).

To calculate the multiplicity of $g \to c\bar{c}$ events in hadronic Z^0 events, $\bar{n}_{g \to c\bar{c}}$, from the results of this fit, we have first to subtract from the measured $g \to D^*$ yield the contribution from $g \to b\bar{b}$ events. Using the measured ratio $B(c \to D^*)/B(b \to D^*) = 1.03 \pm 0.11 \pm 0.10$, we assign $(13.0 \pm 6.2)\%$ (see Table 4) of all gluons as coming from a $g \to b\bar{b}$ event and subtract them from the gluon yield. We then calculate the multiplicity of $g \to c\bar{c}$ events in hadronic Z^0 decays, $\bar{n}_{g \to c\bar{c}}$, by dividing the corrected result of the fit for $F_{g \to Q\bar{Q}} \cdot P_g$ by our measurement for $F_{c\bar{c}} \cdot P_c$ and multiplying with the Standard Model prediction $F_{c\bar{c}} = 0.171$. This calculation depends on the assumption that the product branching ratio P_c is equal for directly produced charm quarks and for charm quarks produced in gluon splitting: $P_g = P_c$. This is expected to be at least approximately true. In addition the potentially competing process, the production of $c\bar{c}$ bound states from gluon splitting, is colour suppressed. The cross section of this process has been calculated theoretically to be about a factor of 100 lower than open charm production [43]. Thus, we find

$$\bar{n}_{g \to c\bar{c}} = 0.044 \pm 0.014 \pm 0.015 \ .$$

Our data therefore seem to favour the inclusion of a non zero component of $g \to D^*$, representing the first experimental signs of this process in e^+e^- collisions. The result is consistent with the

[6] These values have been calculated for $M_{top} = 170$ GeV and $M_{higgs} = 300$ GeV.

[7] We determine $B(b \to D^{*\pm} X)$ by assuming that $(80 \pm 5)\%$ of b quarks produce B^+ or B^0 mesons and using an average of the published values for $B(B \to D^{*\pm} X) = (23.8 \pm 4.1)\%$ [42].

Note that we do not use the PDG value since a slight inconsistency was found in its derivation. The value of $B(c \to D^{*\pm} X)$ is calculated from the above quoted P_c, after correcting for the branching ratios $B(D^* \to D^0\pi) = 0.681 \pm 0.013$ and $B(D^0 \to K\pi) = 0.0401 \pm 0.0014$ (see above). Using these numbers we obtain the quoted value for $B(c \to D^*)/B(b \to D^*) = 1.36 \pm 0.20$.

theoretically expected rates (see Table 4) although somewhat higher. More data and additional studies are needed to further establish this result.

6.3 Comparison with Models of Fragmentation Functions

Monte Carlo programs model the fragmentation of quarks and gluons to observable particles and their subsequent decay into more stable hadrons. Whereas models based on perturbative QCD calculations are used to simulate processes like hard gluon radiation, only phenomenological models exist to describe the hadronisation process. We model the final energy yield of the various hadrons produced by implementing an analytical fragmentation function into the Monte Carlo generator and tuning it to what is being measured experimentally. We test various fragmentation functions in conjunction with the parton shower model of JETSET 7.3. While in Section 6 we have treated the dependence of our results on fragmentation models as a systematic error, we now try to use our results to distinguish between them.

The measured x_{D^*} distribution from charm is fitted with the predictions obtained from these different fragmentation models. The fit employed is the same as described in section 6, except that we do not include the contribution from gluon splitting in the fit, but subtract it from the c-like spectrum. The fit is done only for the seven highest bins in x_{D^*}, starting at $x_{\mathrm{D}^*} = 0.3$ to minimise the influence of events from gluon splitting.

The models used are

Peterson: [15]	$f(z)$	$\propto \left[z \left(1 - \frac{1}{z} - \frac{\epsilon_Q}{(1-z)} \right)^2 \right]^{-1}$
Collins and Spiller: [32]	$f(z)$	$\propto \frac{[\frac{(1-z)}{z} + \frac{(2-z)}{(1-z)}\epsilon_Q](1+z^2)}{(1 - \frac{1}{z} - \frac{\epsilon_Q}{(1-z)})^2}$
Lund symmetric: [33]	$f(z)$	$\propto z^{-1}(1-z)^a \exp(-bm_T^2/z)$
Kartvelishvili: [34]	$f(z)$	$\propto z^{\alpha_q}(1-z)$

The JETSET 7.3 Monte Carlo is used to convert these distributions into spectra in x_{D^*}. The scale parameter used is $\Lambda_{\mathrm{JETSET}} = 320$ MeV. The values of the minimal χ^2 from the fits and the corresponding parameters of the functions are listed in Table 7. The errors quoted are statistical and systematic. The systematic error is evaluated by varying the measured points within their systematic errors and repeating the analysis.

These results indicate that the Peterson and the Lund fragmentation schemes are favoured by our data, though the statistics are not sufficient to exclude the other models. It should be noted that the parameters found for the Lund model are significantly different from those determined from a global event analysis using events from all five flavours [14]. In Figure 10, we show the x_{D^*} distributions for the best fit of the different fragmentation functions, with the measured points superimposed, and the χ^2 between the measured points and the different models.

Function		Fitted Parameter	χ^2	prob. (%)
Peterson	ϵ_c	$0.035 \pm 0.007 \pm 0.006$	5.2	51.3
Lund	a	$1.95\ ^{+0.78}_{-0.53} \pm 0.08$		
	b	$1.58\ ^{+0.64}_{-0.42} \pm 0.06$	3.4	62.3
Collins and Spiller	ϵ_c	$0.065 \pm 0.020 \pm 0.006$	12.1	5.9
Kartvelishvili	α_c	$4.2 \pm 0.5 \pm 0.4$	11.5	7.4

Table 7: Minimal χ^2 and the corresponding parameters of the functions for the comparison of the measured $x_{c\to D^*}$ distribution with different fragmentation models. The errors quoted are the statistical and systematic errors. In the last column the probability corresponding to the listed χ^2 for six (five for Lund) degrees of freedom is shown.

7 Study of Scaling Violations

Scaling violations, i.e. changes in the scaled energy spectrum as a function of the centre-of-mass energy, E_{cm}, are an interesting test of QCD [44]. Because of the increased phase space for gluon emission with increased E_{cm}, quarks and gluons tend to attain a smaller fraction of the total energy available, resulting in smaller scaled energy of the observed hadrons. Since the amount of gluon radiation depends on the QCD scale parameter $\Lambda_{\rm QCD}$, scaling violations allow, in principle, this quantity to be measured. There is, however, another reason for a softening of the scaled energy with increasing E_{cm}, simply from threshold effects. For example, at $E_{cm} = 10$ GeV the minimum x_{D^*} is $2m_{D^*}/E_{cm} \sim 0.4$, whereas at 91 GeV this falls to about 0.04.

For inclusive hadron production, scaling violations have been analysed between $E_{cm} \sim 30$ and 91 GeV [45]. In this case the evolution of both gluons and quarks contribute to the decrease of the average scaled energy. In this paper we will compare the measurement of $c \to D^*$ at Z^0 energies to those at lower energies at DORIS [46], PEP [39, 47, 48] and PETRA [38, 49]. All measurements are expected to be dominated by contributions from $c \to D^*$, with effects from gluon splitting into a $c\bar{c}$ pair being very small. A measurement of the scaling violation for charm production is therefore sensitive to the quark evolution with E_{cm} and provides a probe of parton evolution complementary to the measurements using inclusive hadron spectra.

One experimental problem in performing such an analysis is the low statistics of D^* production at lower energies. Instead of comparing the fragmentation functions themselves, we therefore restrict the analysis to the average scaled energies $\langle x_{c\to D^*} \rangle$. To allow for a meaningful comparison of the results we corrected the measurements at lower energies for several effects:

- initial state radiation: the JETSET 7.3 Monte Carlo is used to remove the smearing in the effective centre of mass energy due to initial state radiation. This correction has been applied to the results in references [38, 39, 46, 47, 49];
- losses due to cuts in the D^* energy: some of the measurements at lower centre of mass did not extrapolate beyond some minimum x_{D^*} cut in forming their average. The QCD shower model JETSET was used to do this correction to the results given in references [49];
- bottom contributions to the D^* spectrum: similarly no attempt was made to remove the $b \to D^*$ contribution in references [39, 49]. This correction is also applied on the basis of studies with the JETSET model.

The corresponding corrections are typically +0.04 for the initial state radiation effects and, for some experiments, +0.05 to account for the extrapolation. Uncertainties in these corrections

are treated as systematic errors in the final values for $\langle x_{c\to D^*}\rangle$. The dependence of $\langle x_{c\to D^*}\rangle$ on the centre of mass energy is shown in Figure 11. We find the average scaled energy to be lower by about 30% at 91 GeV compared with the lowest energy measurements, indicating scaling violations.

These measurements can now be used to study the QCD scale parameter, Λ_{QCD}. Since this determination is sensitive to a special subprocess of the parton evolution, it provides a consistency check of QCD calculations. The principle of the method is to apply a perturbative QCD calculation which is valid down to a certain mass cut-off, and then to assume hadronisation properties below this cut-off which are independent of the centre of mass energy. A meaningful study of scaling violations can then be performed using measurements at centre of mass energies that are significantly larger than this cut-off. To reproduce measurements at Z^0 energies, the cut-off used in $\mathcal{O}(\alpha_s^2)$ matrix element calculations must be rather high, $\sim$ 15-20 GeV (see, for example, reference [50]). This implies that measurements at $E_{cm} = 10$ GeV/c^2 cannot be used. This reduces the lever arm for the $\Lambda_{\overline{MS}}$ determination significantly and little sensitivity can be obtained. QCD shower models, based on the leading log approximation, use cut-offs of $\sim$ 1 GeV/c^2. They therefore allow a reasonably precise determination of the QCD scale parameter. However, since these results depend on model assumptions, they are specific to the model used. We refer to the corresponding values as 'Λ_{MODEL}'.

In a first step we compare the measurements to the QCD shower model JETSET 7.3. In Figure 11 the expected energy dependence is shown for values of $\Lambda_{\mathrm{JETSET}}$ between 0 GeV [8] and 1 GeV. For this analysis we use a Peterson fragmentation function within JETSET and tune the parameter ϵ_c to give $\langle x_{c\to D^*}\rangle = 0.515$ for $E_{cm} = M_{Z^0}$. The ϵ_c parameter varies between 0.2 and $2{\cdot}10^{-5}$ for this range of $\Lambda_{\mathrm{JETSET}}$. As expected, the energy variation increases with increasing $\Lambda_{\mathrm{JETSET}}$. Even at $\Lambda_{\mathrm{JETSET}} = 0$ GeV/c^2 a significant variation of $\langle x_{c\to D^*}\rangle$ with energy is observed, illustrating the above mentioned threshold effects.

A fit to the measurements yields $\Lambda_{\mathrm{JETSET}} = 180^{+200}_{-90}$ MeV with a χ^2 of 4.0 for 2 degrees of freedom. This value is in agreement with $\Lambda_{\mathrm{JETSET}} = 310\pm30$ MeV obtained by fitting the event properties at the fixed centre of mass energy of 91.2 GeV [51]. The error on the measured value includes the statistical error at 91.2 GeV.

We repeat the analysis using the ARIADNE model [35]. We obtain $\Lambda_{\mathrm{ARIADNE}} = 150^{+80}_{-70}$ MeV. This value is again consistent with the 200 ± 20 MeV obtained by fitting event properties at E_{cm}= 91.2 GeV [14]. The χ^2 is 3.2 for 2 degrees of freedom in this case.

These determinations of Λ_{MODEL}, while statistically not competitive with the determination from inclusive event shapes, can be interpreted as consistency checks of QCD, indicating that the models JETSET and ARIADNE describe this special process with the same parameters as obtained from much more inclusive measurements.

A study of scaling violations of $c \to D^*$ production in the HERWIG model is hampered by its rather inflexible hadronisation scheme which makes it difficult to tune the mean scaled energy to the value observed in this analysis. Using the model parameters optimised to describe the OPAL measurements of event shapes [52], we find the HERWIG prediction to be $\langle x_{D^*}\rangle = 0.487$ at $E_{cm} = 91.16$ GeV/c^2. The energy variation of $\langle x_{D^*}\rangle$ between $E_{cm} = 10$ and $E_{cm} = 91.16$ GeV/c^2 as predicted by HERWIG is less than the one actually observed, leading to a χ^2 of 11.1 for two degrees of freedom.

[8] For technical reasons Λ was not set exactely to zero, but a value $\Lambda_{\mathrm{JETSET}} = 0.005$ GeV was used.

8 Conclusions

We have studied the production of D^* mesons in Z^0 decays, based on a sample of 1969 fully reconstructed events. We identify $Z^0 \to b\bar{b}$ decays in the sample using a number of b tagging methods.

We have measured the total multiplicity of charged D^* mesons in multihadronic decays of the Z^0 to be

$$\bar{n}_{Z^0 \to D^{*\pm} X} = 0.183 \pm 0.009 \pm 0.007 \pm 0.008 \ .$$

Here the first error quoted is the statistical error, the second one the systematic error of this analysis, and the third error due to the uncertainty in the branching ratios $B(D^* \to D^0\pi)$ and $B(D^0 \to K\pi)$. For this measurement we have summed over both charged states of the D^* meson.

Using the flavour separation methods we have investigated the scaled energy spectra of D^* mesons in primary b and c decays and from gluon splitting. We find the product branching ratios for the production of D^* mesons in $c\bar{c}$ and $b\bar{b}$ events and their subsequent decay $D^* \to D^0\pi$, $D^0 \to K\pi$ to be

$$\begin{aligned} \Gamma_{b\bar{b}}/\Gamma_{had} \cdot B(b \to D^*) \cdot B(D^* \to D^0\pi) \cdot B(D^0 \to K\pi) &= (1.24 \pm 0.10 \pm 0.09) \cdot 10^{-3} \\ \Gamma_{c\bar{c}}/\Gamma_{had} \cdot B(c \to D^*) \cdot B(D^* \to D^0\pi) \cdot B(D^0 \to K\pi) &= (1.006 \pm 0.055 \pm 0.061) \cdot 10^{-3} \end{aligned}$$

where $\Gamma_{q\bar{q}}/\Gamma_{had} \equiv \Gamma(Z^0 \to q\bar{q})/\Gamma(Z^0 \to \text{hadrons})$. From these measurements we find the partial width for a Z^0 into $c\bar{c}$ to be

$$\frac{\Gamma(Z^0 \to c\bar{c})}{\Gamma(Z^0 \to \text{hadrons})} = 0.142 \pm 0.008 \pm 0.009 \pm 0.011 \ ,$$

where the last error quoted is due to the branching ratios used. Alternatively, using the Standard Model predictions for $\Gamma_{b\bar{b}}/\Gamma_{had}$ and $\Gamma_{c\bar{c}}/\Gamma_{had}$, we find the production rate for D^* mesons in c decays relative to that in b decays to be

$$\frac{B(c \to D^*)}{B(b \to D^*)} = 1.03 \pm 0.11 \pm 0.10 \ .$$

We find indications that the process $g \to c\bar{c} \to D^*$ contributes to our sample and measure the multiplicity of such events in multihadronic decays of the Z^0 to be

$$\bar{n}(g \to c\bar{c}) = 0.044 \pm 0.014 \pm 0.015 \ ,$$

assuming the Standard Model prediction for $\Gamma_{c\bar{c}}/\Gamma_{had}$. This result is consistent with theoretical expectations. The errors quoted are the statistical and the systematic error.

The mean scaled energy of D^* mesons in $c\bar{c}$ decays is measured to be

$$\langle x_{c \to D^*} \rangle = 0.515^{+0.008}_{-0.005} \pm 0.010 \ .$$

The error quoted includes a component to take possible model dependencies of this measurement into account.

Comparing the measured x_{D^*} spectrum to different analytical fragmentation functions we find that the Lund and the Peterson fragmentation functions are favoured compared to the other models.

Evidence for scaling violations is observed by comparing our measured $\langle x_{c \to D^*} \rangle$ with that found at lower energies. The values of the QCD scale parameter Λ derived from these scaling violations for the JETSET and ARIADNE models are found to be in good agreement with those obtained from measurements of the event shapes at Z^0 energies.

Acknowledgements:

It is a pleasure to thank the SL Division for the efficient operation of the LEP accelerator, the precise information on the absolute energy, and their continuing close cooperation with our experimental group. We wish to thank P. Zerwas and B. Kniehl for their help in analysing the gluon contribution and M. Seymour for useful comments and discussions. In addition to the support staff at our own institutions we are pleased to acknowledge the
Department of Energy, USA,
National Science Foundation, USA,
Texas National Research Laboratory Commission, USA,
Science and Engineering Research Council, UK,
Natural Sciences and Engineering Research Council, Canada,
Fussefeld Foundation,
Israeli Ministry of Energy and Ministry of Science,
Minerva Gesellschaft,
Japanese Ministry of Education, Science and Culture (the Monbusho) and a grant under the Monbusho International Science Research Program,
German Israeli Bi-national Science Foundation (GIF),
Direction des Sciences de la Matière du Commissariat à l'Energie Atomique, France,
Bundesministerium für Forschung und Technologie, Germany,
National Research Council of Canada,
A.P. Sloan Foundation and Junta Nacional de Investigacão Científica e Tecnológica, Portugal.

Appendix A: The Neural Network Technique

In this Appendix we briefly introduce the variables used in the artificial neural network (ANN) presented in Section 5.2. They are similar to those used in another analysis [24]. For training and implementation of the network we have used the program JETNET described in [53]. In general these variables are constructed to maximise the information contained in the different mass and fragmentation hardness of b jets compared to those from lighter flavours. Charged tracks and unassociated clusters are used to calculate the following seven jet shape variables :

- $\mathcal{B}_{jet}$: The boosted sphericity of the jet. The particles of a jet are boosted in the direction opposite to the jet momentum vector with $\beta = 0.95$, corresponding to a boost into the rest frame of a mean b jet. The sphericity [14] of the jet is calculated in this new frame.

- $(p_{t,tot})^2$: The sum of the square of the transverse momenta of all particles belonging to the jet,

$$(p_{t,tot})^2 = \sum_i p_{t_i}^2 \quad ,$$

  where i runs over all particles in the jet.

- p_l^l : The longitudinal momentum of the leading particle with respect to the jet axis, where the leading particle is defined as the most energetic particle of the jet.

- p_t^l : The transverse momentum of the leading particle with respect to the jet axis.

- p_{lt}^{norm} : The normalised product of the sum of the transverse momenta and the sum of longitudinal momenta of all particles of the jet,

$$p_{lt}^{norm} = \frac{\sum_i p_{t_i} \cdot \sum_i p_{l_i}}{\sum_i p_i^2} \quad ,$$

  where i runs over all particles of the jet.

- $\mathcal{D}_{123}$: The directed sphericity formed by the three most energetic particles of the jet,

$$\mathcal{D}_{123} = \frac{\sum_{i=1}^{3} \tilde{p}_{t_i}^2}{\sum_{i=1}^{3} \tilde{p}_i^2} \quad ,$$

  where $\tilde{p}_i$ refers to the momentum of particle i in the rest frame of the three most energetic particles, and $\tilde{p}_{t_i}$ is the transverse momentum calculated with respect to the jet axis in the laboratory frame. The index i runs over the three most energetic particles of the jet.

- $\mathcal{M}_{123}$: The invariant mass of the three most energetic particles of the jet.

We use an ANN of the feed forward type, trained with the back-propagation algorithm [23], to separate $b\bar{b}$ events from others. The ANN consists of three layers with seven inputs, seven nodes in the hidden layer and one output node. After the training procedure described in the text, which relies on data for training in $b\bar{b}$ events, we achieve a performance of the net of 65.2%. The performance is defined as the ratio of correctly identified $b\bar{b}$ or $c\bar{c}$ events to all events in a sample of events consisting of 50% $c\bar{c}$ events and 50% $b\bar{b}$ events.

References

[1] Particle Data Group, *Review of Particle Properties*, Phys. Rev. **D 50** (1994) 1173.

[2] B. Mele and P. Nason, Phys. Lett. **B 245** (1990) 635; Nucl. Phys. **B 361** (1991) 626.
G. Colangelo, B. Nason *A Theoretical study of the c and b fragmentation function from* e^+e^- *annihilation.* Frascati LNF**92-017** P.
R.L. Jaffe, L. Randall, *Heavy quark fragmentation into heavy mesons.* Nucl.Phys. **B 412** (1994) 79.

[3] Yu. Dokshitzer, V. Khoze and S. Troyan, *Specific features of heavy quark fragmentation. I. Leading quarks.* Lund preprint LU TP **92/10** (1992);
Yu. Dokshitzer, Lectures at the International School of Subnuclear Physics, Erice, July 1993.

[4] OPAL Collaboration, G. Alexander *et al.*, Phys. Lett. **B 262** (1991) 341.

[5] OPAL Collaboration, R. Akers *et al.*, Z. Phys. **C 60** (1993) 601.

[6] OPAL Collaboration, K. Ahmet *et al.*, Nucl. Instr. Meth. **A 305** (1991) 275.

[7] P.P. Allport *et al.*, Nucl. Instr. Meth. **A 324** (1993) 34.

[8] O. Biebel *et al.*, Nucl. Instr. Meth. **A 323** (1992) 169.

[9] M. Hauschild *et al.*, Nucl. Instr. Meth. **A 314** (1992) 74.

[10] OPAL Collaboration, G. Alexander *et al.*, Z. Phys. **C 52** (1991) 175.

[11] JADE Collaboration, W. Bartel *et al.*, Z. Phys. **C 33** (1986) 23;
JADE Collaboration, S. Bethke *et al.*, Phys. Lett **B 213** (1988) 235.

[12] OPAL Collaboration, P.D. Acton *et al.*, Z. Phys. **C 59** (1993) 183.

[13] T. Sjöstrand, Comp. Phys. Comm. **39** (1986) 347;
M. Bengtsson and T. Sjöstrand, Comp. Phys. Comm. **43** (1987) 367;
T. Sjöstrand, Int. J. of Mod. Phys. **A 3** (1988) 751.

[14] OPAL Collaboration, M.Z. Akrawy *et al.*, Z. Phys. **C 47** (1990) 505.

[15] C. Peterson *et al.*, Phys. Rev. **D 27** (1983) 105.

[16] J. Allison *et al.*, Nucl. Instr. Meth. **A 317** (1991) 47.

[17] OPAL Collaboration, P.D. Acton *et al.*, Z. Phys. **C 58** (1993) 523.

[18] OPAL Collaboration, M.Z. Akrawy *et al.*, Z. Phys. **C 55** (1992) 191.

[19] OPAL Collaboration, P.D.Acton *et al.*, Phys. Lett. **B 307** (1993) 247.

[20] ALEPH Collaboration, D. Buskulic *et al.*, Phys. Lett. **B 307** (1993) 194.

[21] CLEO Collaboration, J. Bartelt *et al.*, Phys. Rev. Lett. **71** (1993) 1680.

[22] OPAL Collaboration, R. Akers *et al.*, Z. Phys. **C 60** (1993) 199.

[23] For an introduction to neural networks see: D.E. Rumelhart, G.E. Hinton and R.J. William *Learning Representation by Backpropagating Errors.* Nature **323** (1986) 533;
a comprehensive review of neural networks and their application in high energy physics may be found in: C. Peterson, T. Rögnvaldsson, in *1991 CERN School of Computing.* ed. C. Verkerk, CERN Report **92/02** (1992).

[24] ALEPH Collaboration, D. Buskulic *et al.*, Z. Phys. **C 62** (1994) 1.

[25] OPAL Collaboration, R. Akers *et al.*, Z. Phys. **C 61** (1994) 357.

[26] DELPHI Collaboration, P. Abreu *et al.*, Z. Phys. **C 59** (1993) 533.

[27] ALEPH Collaboration, D. Decamp *et al.*, Phys. Lett. **B 244** (1990) 551;
ALEPH Collboration, D. Decamp *et al.*, Phys. Lett. **B 266** (1991) 218;
DELPHI Collaboration, P. Abreu *et al.*, Z. Phys. **C 56** (1992) 47.

[28] CLEO Collaboration, S. Henderson *et al.*, Phys. Rev. Lett. **D45** (1992) 2212;
M. Morris, PhD. Thesis, Cornell University, (1991) (unpublished);
DELCO Collaboration, W.Bacino *et al.*, Phys. Rev. Lett. **43** (1979) 1073;
G.Altarelli *et al.*, Nucl. Phys. **B 264** (1991) 219;
N. Isgur, D. Scora, B. Grinstein and M. Wise, Phys. Rev. **D 39** (1989) 799.

[29] I.I. Bigi, N.G. Uraltsev, Phys. Lett. **B280** (1992) 271.

[30] OPAL Collaboration, R. Akers *et al.*, Z. Phys. **C 61** (1994) 209.

[31] M.H. Seymour, *Heavy Quark Pair Multiplicity in e^+e^- Events*, Lund preprint LU TP **94/7** (1994).

[32] P. Collins and T. Spiller, J. Phys. **G 11** (1985) 1289.

[33] B. Andersson, G. Gustafson, B. Söderberg, Z. Phys. **C 20** (1983) 317;
M.G. Bowler, Z. Phys. **C 11** (1981) 169;
D.A. Morris, Nucl. Phys. **B 313** (1989) 634.

[34] V.G. Kartvelishvili, A.K. Likehoded, V.A. Petrov. Phys. Lett. **B 78** (1978) 615.

[35] L. Lönnblad, Comp. Phys. Comm. **71** (1992) 15.

[36] CLEO Collaboration, D. Bortoletto *et al.*, Phys. Rev. **D 37** (1988) 1719.

[37] P. Mättig, Phys. Rep. **177** (1989) 141.

[38] TASSO Collaboration, W. Braunschweig *et al.*, Z. Phys. **C 44** (1989) 365.

[39] HRS Collaboration, P. Baringer *et al.*, Phys. Lett. **B 206** (1988) 551.

[40] CLEO Collaboration, M. Athanas *et al.*, *Semileptonic branching fractions of charged and neutral* B *mesons.* Cornell report CLNS **94/1286** (1994).

[41] Calculated using the ZFITTER program described in:
D. Bardin *et al.*, CERN-TH **6443/92** (1992) 1;
D. Bardin *et al.*, Phys. Lett. **B 255** (1991) 290;
D. Bardin *et al.*, Nucl. Phys. **B 351** (1991) 1;
D. Bardin *et al.*, Z. Phys. **C 44** (1989) 493.

[42] ARGUS Collaboration, H. Albrecht *et al.*, Z. Phys. **C 52** 353 (1991);
CLEO Collaboration, D. Bortoletto *et al.*, Phys.Rev **D 45** (1992) 31.

[43] K. Hagiwara, A.D. Martin and W.J. Stirling, Phys. Lett. **B 267** (1991) 527;
and erratum in Phys. Lett. **B 316** (1993) 631.

[44] See e.g. G. Altarelli, Phys. Rep. **81** (1982) 1.

[45] DELPHI Collaboration, P. Abreu *et al.*, Phys Lett. **B 311** (1993) 40.

[46] ARGUS Collaboration, H. Albrecht *et al.*, Z. Phys. **C 52** (1991) 353
and R. Mankel private communication.

[47] DELCO Collaboration, H. Yamamoto *et al.*, Phys. Rev. Lett. **54** (1985) 522.

[48] TPC/Two-Gamma Collaboration, H. Aihara *et al.*, Phys. Rev. **D 34** (1986) 1945.

[49] JADE Collaboration, W. Bartel *et al.*, Phys. Lett. **B 146** (1984) 121.

[50] OPAL Collaboration, P. Acton *et al.*, Z. Phys. **C 55** (1992) 1.

[51] OPAL Collaboration, P. Acton *et al.*, Z. Phys. **C 58** (1993) 387.

[52] G. Marchesini *et al.*, Comp. Phys. Comm. **76** (1992) 465.

[53] L. Lönnblad *et al.*., Comp. Phys. Commun. **81** (1994) 185.

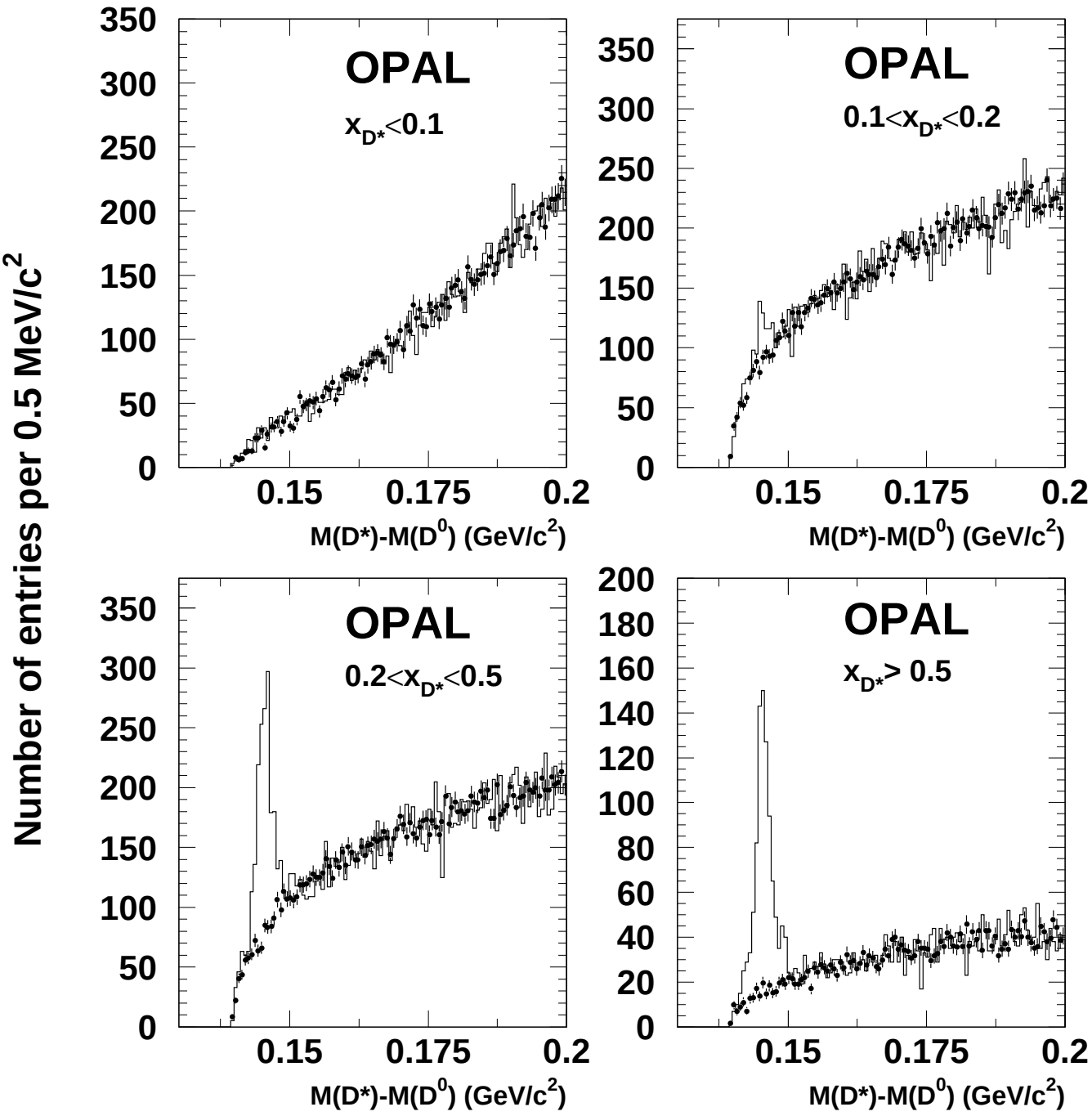

Figure 1: The distributions of the difference of the invariant mass between the D^* candidate and the D^0 candidate, in four ranges of x_{D^*}. The line histograms show the signal sample, and the points show the distributions of the background estimator obtained from wrong charge, reflected pion and reflected pion wrong charge combinations (see text for further explanations).

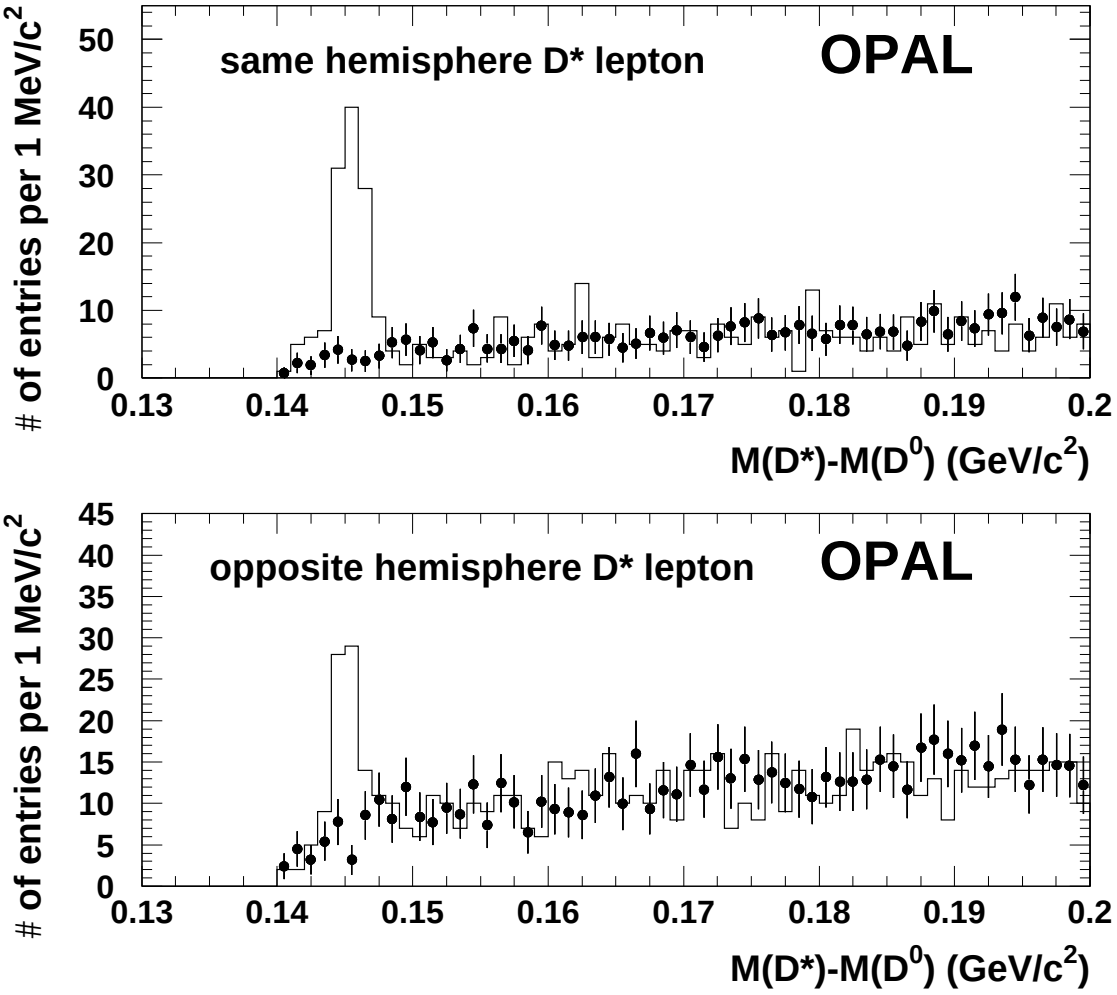

Figure 2: The distribution of the difference of the invariant mass between the D^* candidate and the D^0 candidate, after having applied the M_{D^0} cut, for the $D^*\ell$ and D^*/ℓ candidate samples. The line histograms show the signal sample, and the points show the distribution of the background estimator obtained from wrong charge, reflected pion and reflected pion wrong charge combinations, with leptons of all charge.

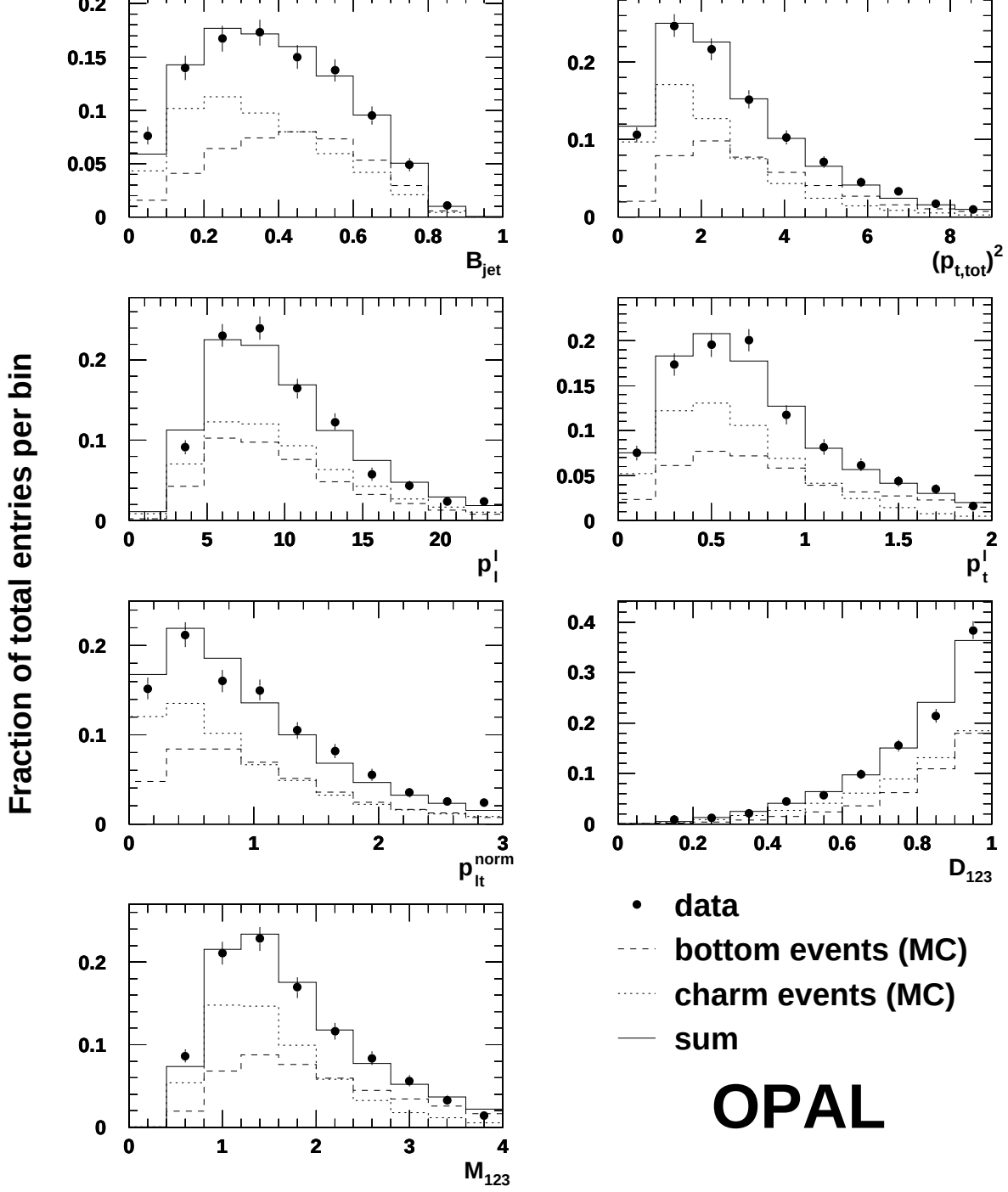

Figure 3: The distributions of the seven jet shape variables used as an input for the neural network. Shown are the D^* candidates (points with error bars), the $b\bar{b}$ training and test events (dashed line), and the $c\bar{c}$ training and test events (dotted line). In each case the full histogram is the sum of the $b\bar{b}$ and the $c\bar{c}$ training and test events, with the distribution to unit area. The contributions of the $b\bar{b}$ and $c\bar{c}$ events are weighted according to their normalisation measured with the ANN.

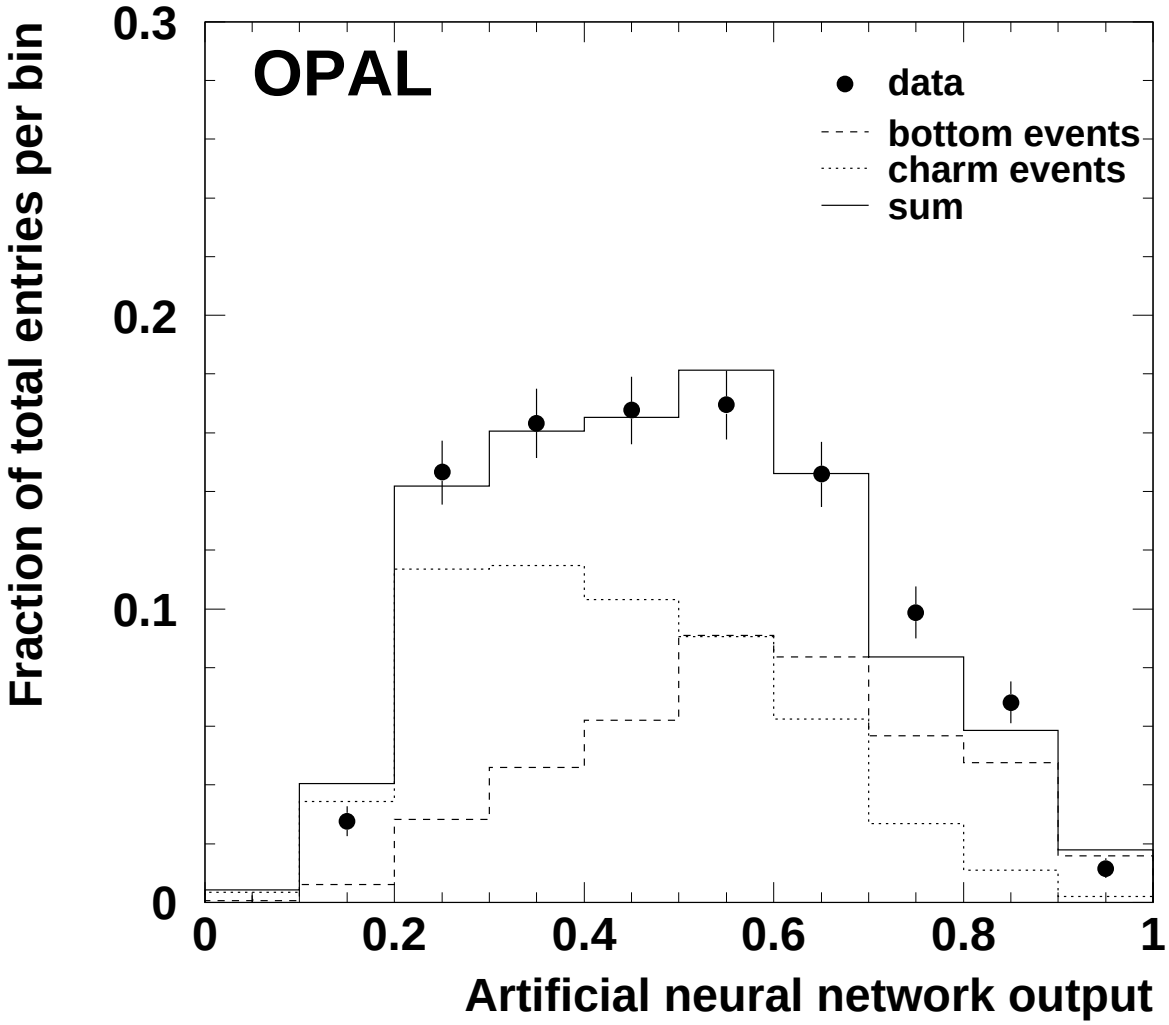

Figure 4: The normalised distribution of the neural network output for the D^* candidates (points with error bars), for the $b\bar{b}$ training and test events (dashed line), and for the $c\bar{c}$ training and test events(dotted line). The full histogram is the sum of the $b\bar{b}$ and the $c\bar{c}$ training and test events. The contributions of the $b\bar{b}$ and $c\bar{c}$ events are weighted according to their normalisation measured with the ANN.

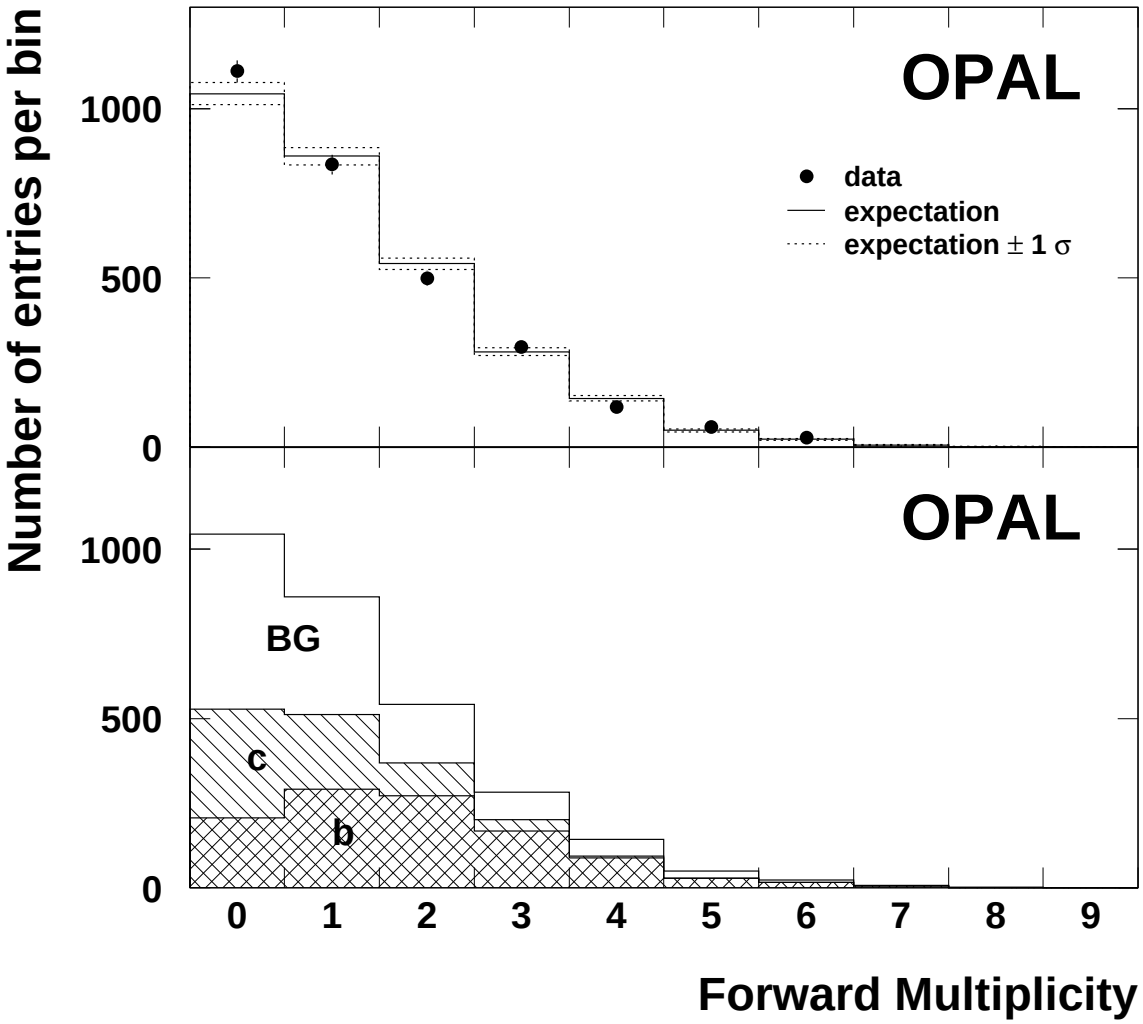

Figure 5: The forward multiplicity distributions for the data (points with error bars) are shown along with the expectation. The expected forward multiplicity spectrum is calculated as the sum of the background (BG) as estimated from the data, and the Monte Carlo b $\rightarrow$ D^* and c $\rightarrow$ D^* contributions fixed to the levels found using the forward multiplicity separation only. In the upper plot, the dotted lines are the errors on the expected distribution, due primarily to the background statistics. The lower plot shows the expected contribution from each of the three distinct sources.

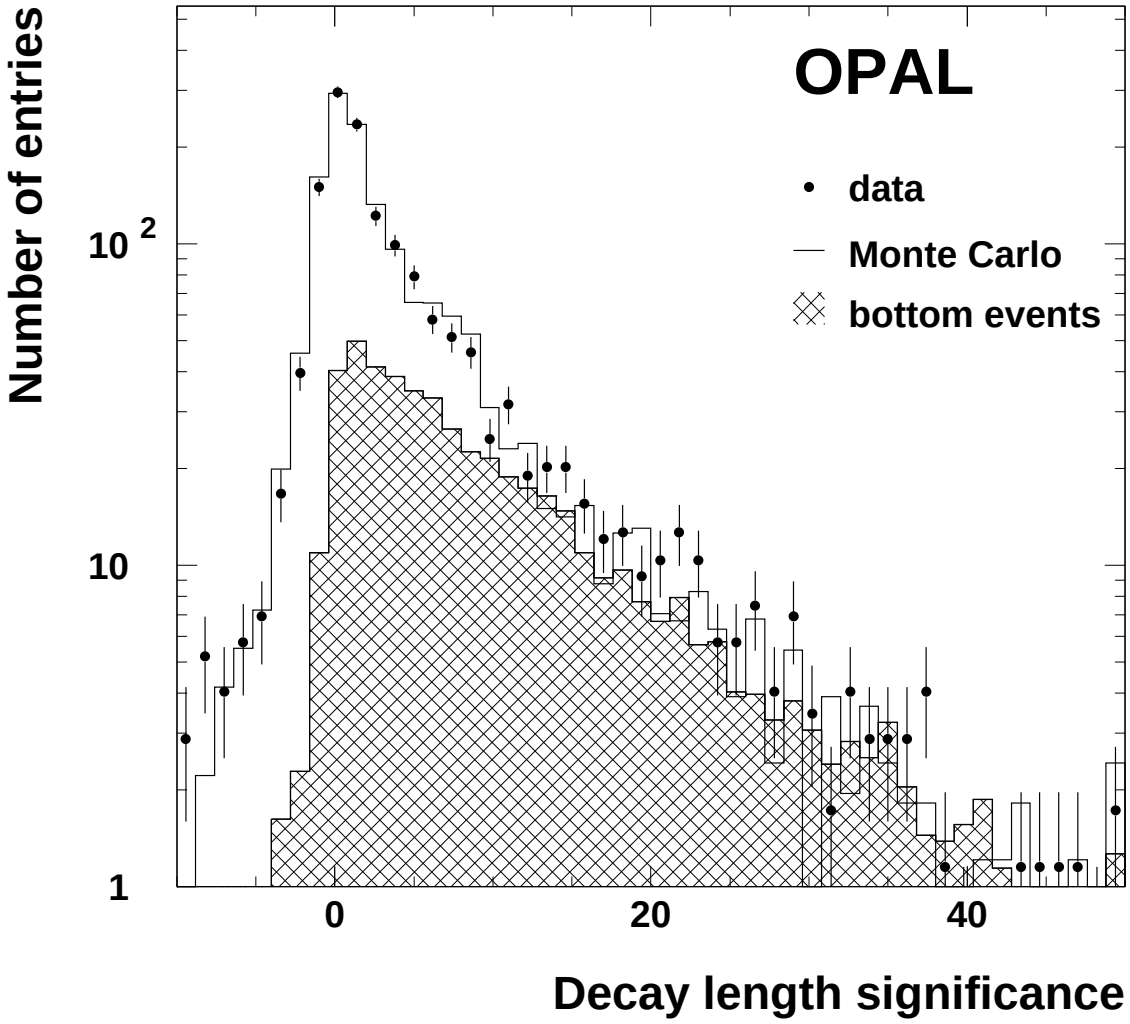

Figure 6: The distribution of decay length significance, D, for D^* candidates. The points are data, and the line histogram is Monte Carlo. The hatched histogram is the contribution from b-quarks as predicted by the Monte Carlo normalised according to the result of the analysis.

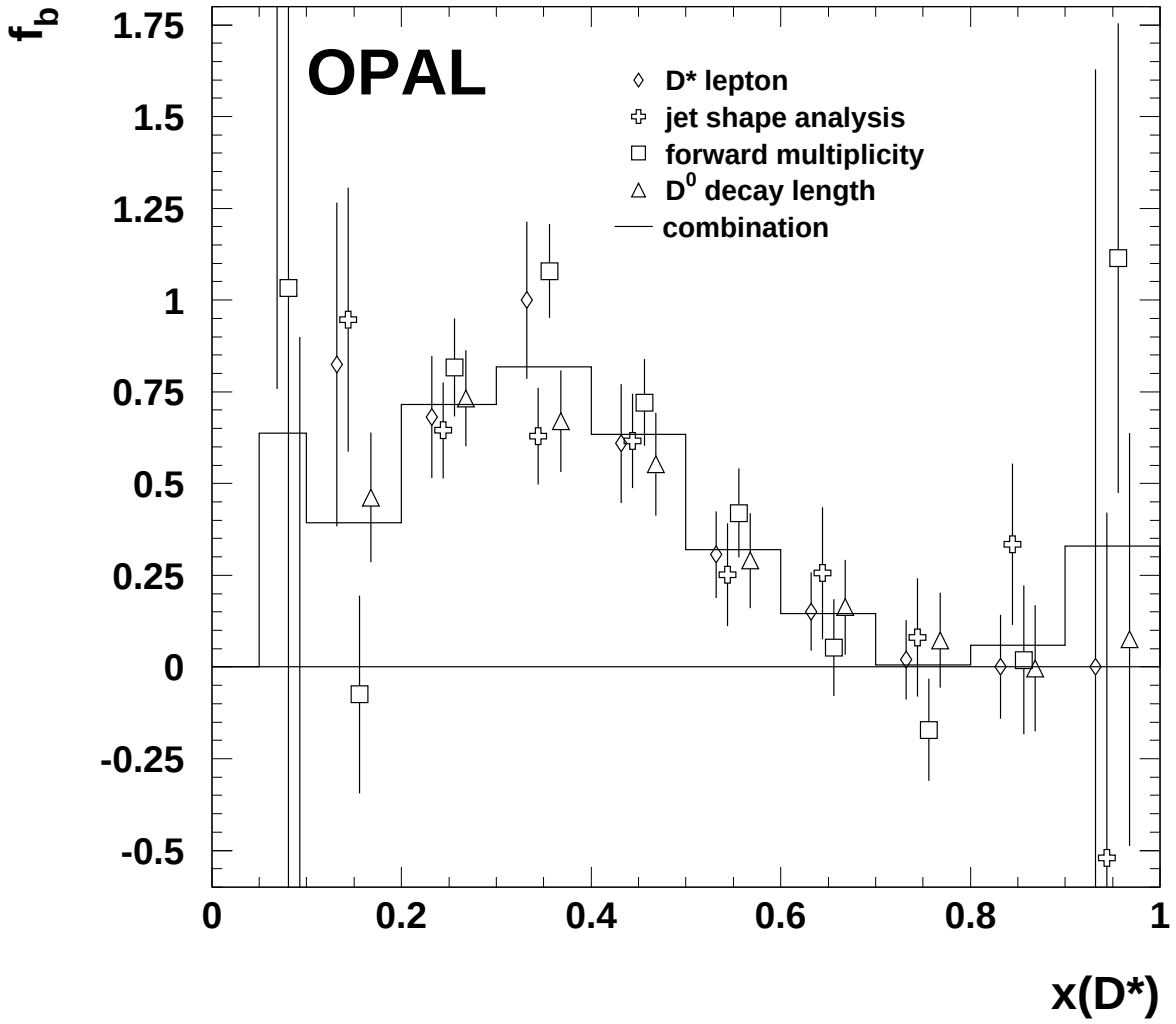

Figure 7: The reconstructed fraction, f_{b}, of D^* mesons from b decays in multihadronic Z^0 decays, as a function of x_{D^*}. The points are the results of the individual analyses and the combination is shown by the solid line. For clarity the individual points have been slightly shifted in x_{D^*}. The errors shown are the combined statistical and systematic errors.

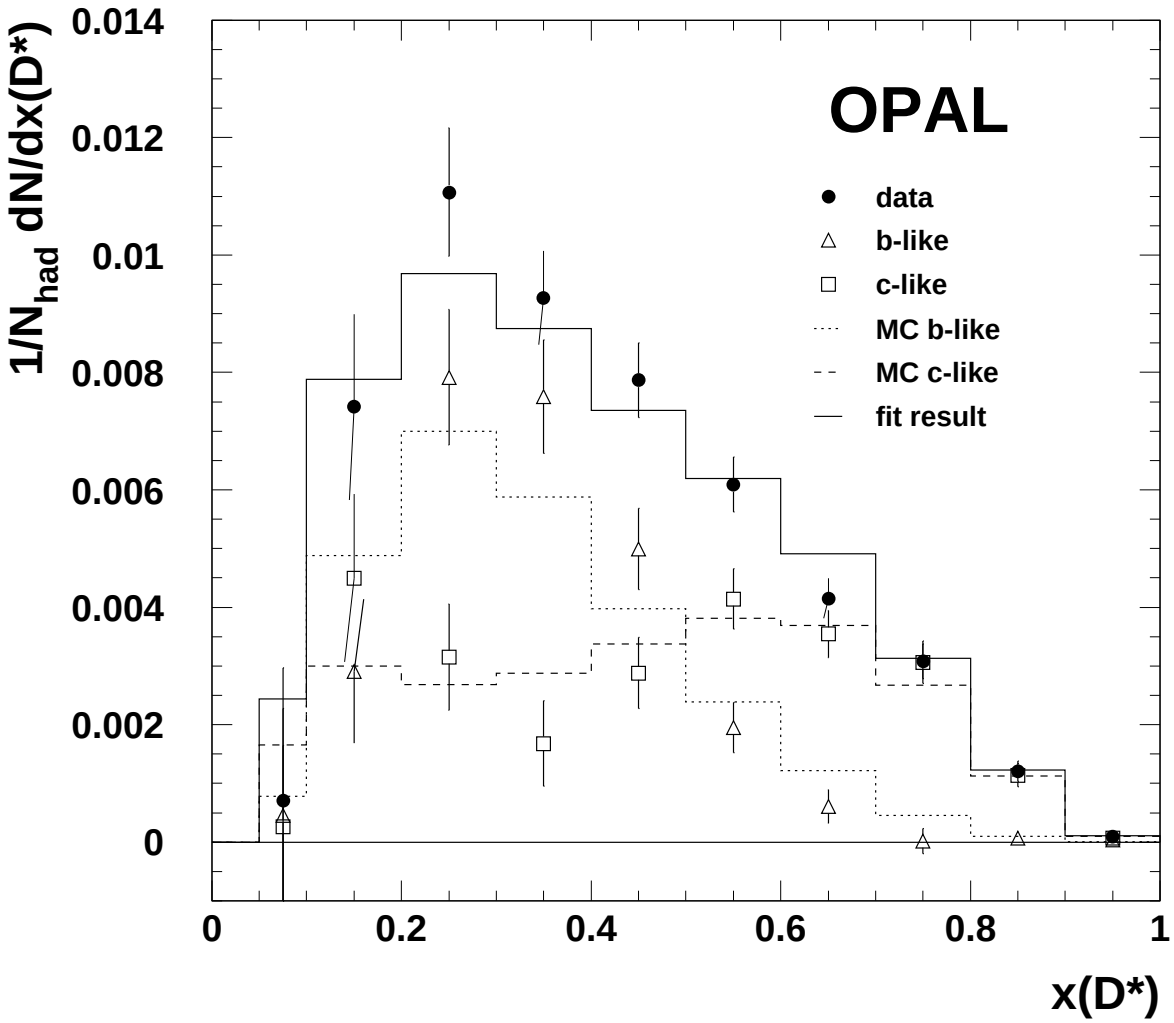

Figure 8: The observed yield of D^* mesons normalised to the total number of multihadronic events, as a function of x_{D^*}. The filled points are the total measured yield, the open squares represent the contribution from c decays, and the open triangles represent the measured contribution from b decays. The errors shown include both statistical and systematic contributions. The superimposed histograms are the predictions from Monte Carlo for $c \to D^*$ and $g \to D^*$ contributions combined (dashed line) and that from b decays (dotted line) with parameters as determined in the analysis.

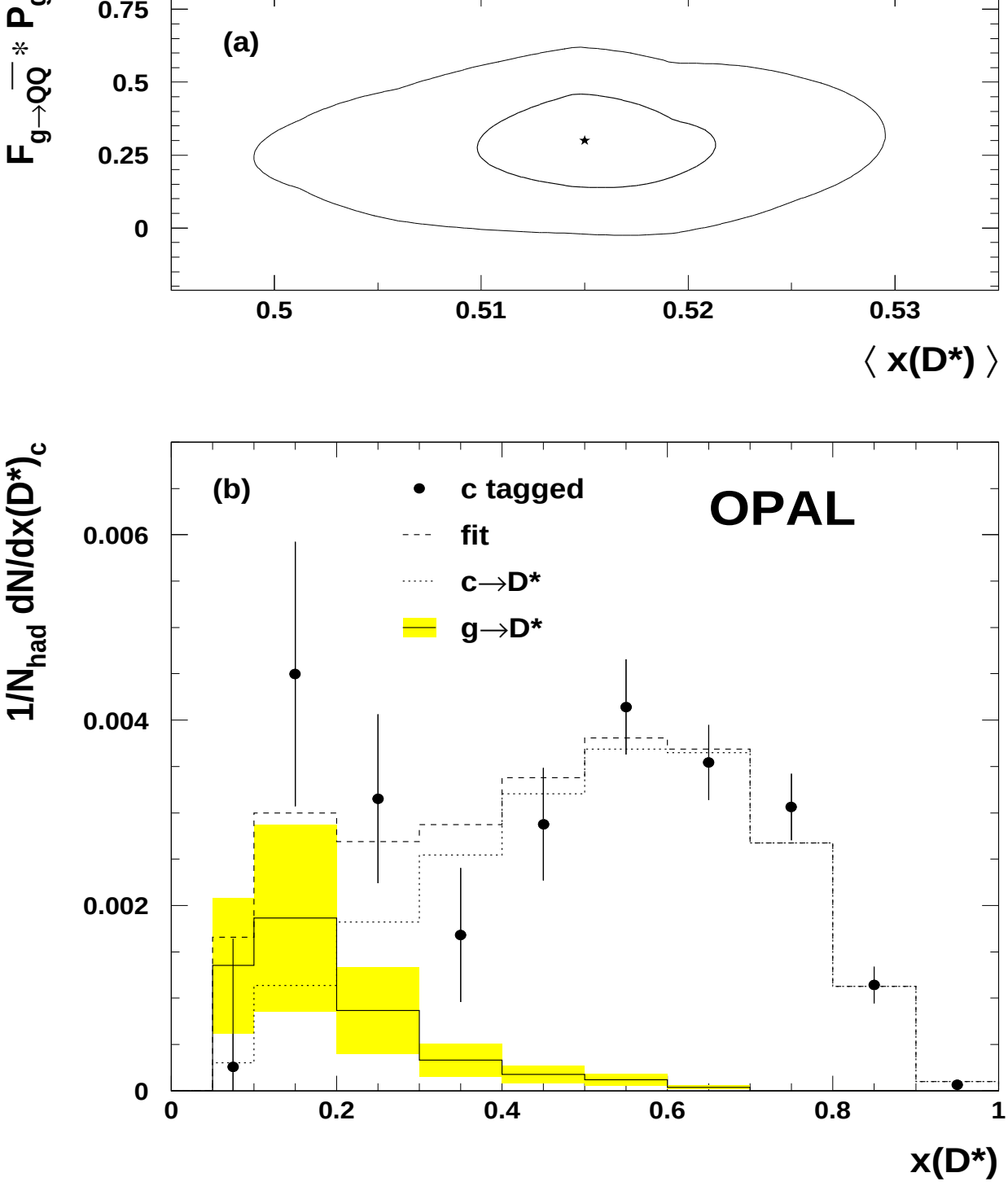

Figure 9: (a) The χ^2 contours for one and two standard deviations in the $\langle x_{c\to D^*}\rangle$ versus $F_{g\to Q\bar{Q}} \cdot P_g$ plane, where $P_g = B(Q \to D^*) \cdot B(D^* \to D^0\pi) \cdot B(D^0 \to K\pi)$. Here $F_{g\to Q\bar{Q}}$ is the fraction of Z^0 decays producing a heavy quark pair (c or b) from gluon splitting.
(b) The observed yield of D^* mesons in c-tagged events, normalised to the total number of multihadronic events. The dashed curve is the result from the a allowing both quark and gluon contributions to vary. The dotted line is the $c \to D^*$ component, and the solid one indicates the component from gluon splitting. The errors on the latter have been indicated by the shaded area, superimposed on the $g \to D^*$ curve.

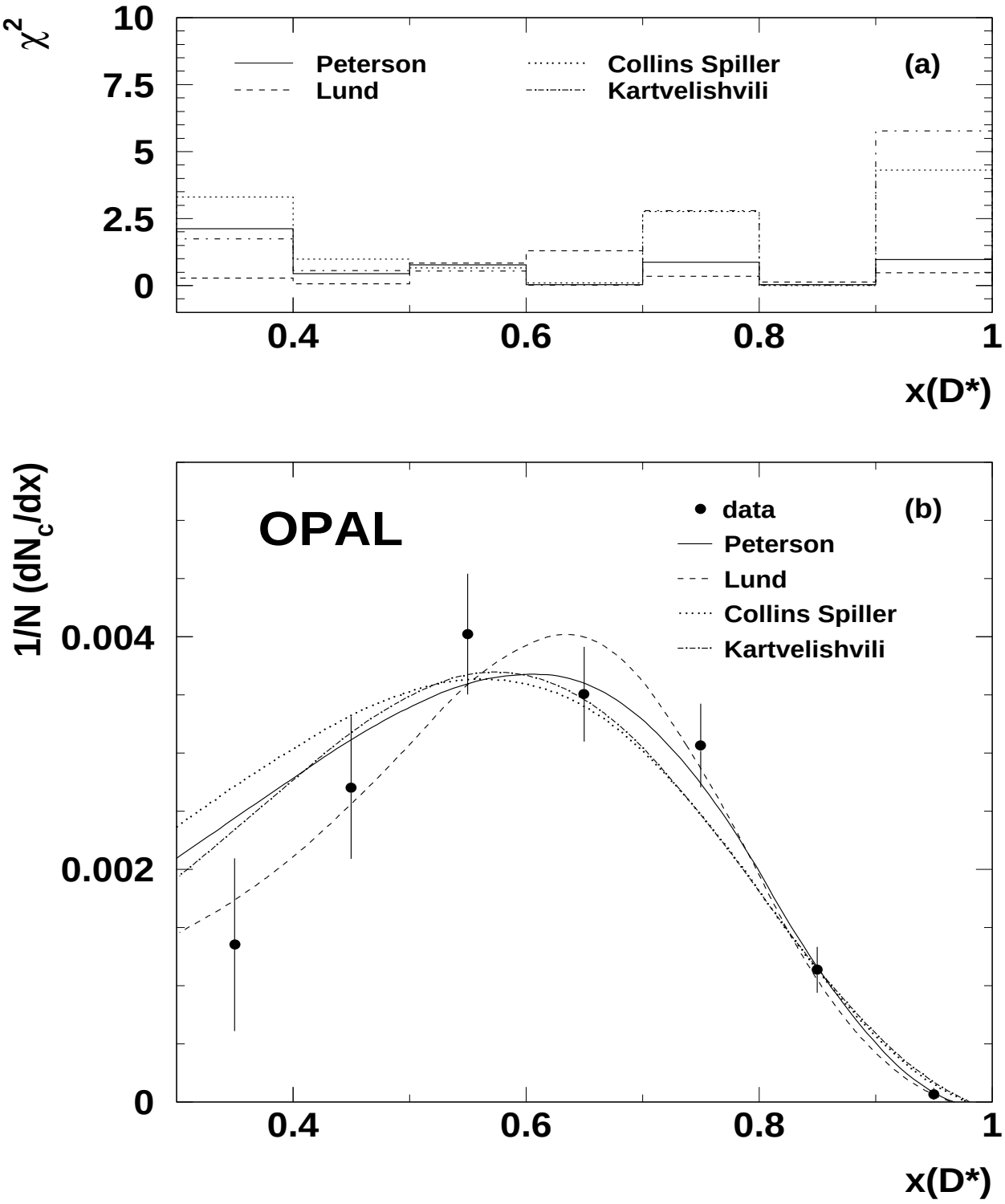

Figure 10: The D* energy spectra as predicted by different models, compared to the observed yield of D* mesons in c-tagged events. (a) The χ^2 for each model at each value of x_{D^*} is shown. (b) The curves shown for each model correspond to those parameters giving the best fit to the data points.

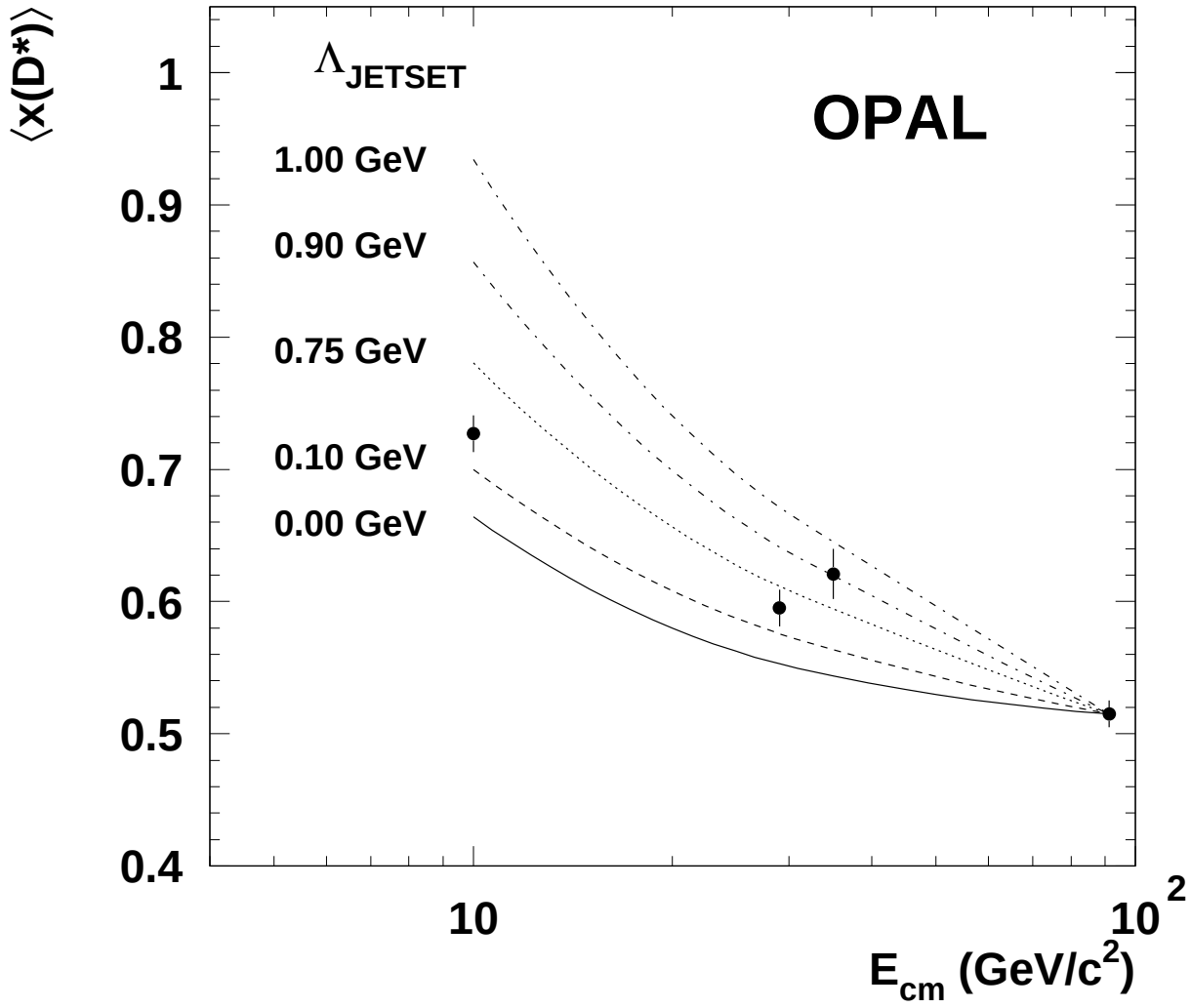

Figure 11: The measured average scaled energy of the D^* for centre of mass energies between 10 and 91.16 GeV (points). Also shown are the JETSET expectations for various values of the QCD scale $\Lambda_{\rm JETSET}$. The curves represent the expectations for Λ =0, 0.1, 0.5, 0.9 and 1 GeV. The hadronisation parameter ϵ_c of each curve is chosen such that the average $x_{\rm D^*} = 0.515$ at 91.16 GeV.